

REVIEWS OF MODERN PHYSICS

VOLUME 39, NUMBER 4

OCTOBER 1967

Elements of the Brueckner–Goldstone Theory of Nuclear Matter*

B. D. DAY

Argonne National Laboratory, Argonne, Illinois

The basic ideas of the Brueckner–Goldstone theory of nuclear matter are presented in a simple way. The treatment is aimed at beginners and nonspecialists. It is supposed to provide the necessary background for the review article by Bethe and Rajaraman which follows this paper. Therefore, the discussion is limited to a few important topics, and these are considered in some detail.

The Goldstone expansion is presented (but not derived) and the construction and evaluation of the Goldstone diagrams are explained. The reaction matrix and the correlated two-body wave function are defined, and their properties are discussed. The reference-spectrum method for calculating the reaction matrix is derived, and its use is illustrated. Finally, the related topics of convergence and the definition of single-particle energies are considered. The choice of the single-particle potential energy for occupied states is treated in detail. (Intermediate-state energies will be discussed by Bethe and Rajaraman.) The reason for the divergence of the perturbation series for the binding energy is exhibited; and this series is rearranged into a convergent expansion, for which the density plays the role of small parameter.

I. INTRODUCTION

The theory of nuclear matter, which was initiated by Brueckner¹ over ten years ago, seems now to be in a satisfactory state. The necessary many-body theory is understood, and it appears likely that good agreement between theory and experiment will be obtained (a calculation with the best available nucleon–nucleon force has not yet been completed, however). It is therefore appropriate to present the methods and results of the theory in a form which will be useful to interested physicists who have not specialized in the study of nuclear matter.² This article is an attempt to explain the basic ideas of the theory in an understandable way.

Before starting on the formalism, let us briefly consider the relationship between the theory of nuclear matter and nuclear physics as a whole. The main aim of nuclear physics is to understand the structure of nuclei in terms of their elementary constituents and the interactions among them. Thus one should in principle start from a fundamental theory of nucleons and derive the existence and properties of all real nuclei. However, no such fundamental theory is available,

and even if it were, it would probably contain virtual mesons, nucleon–antinucleon pairs, etc., and would be very hard to calculate with. So in order to treat nuclei, we have to take some sort of nonrelativistic limit of the fundamental theory and use *this* as a starting point. We do not know what this nonrelativistic limit is, and we must therefore make a guess. The usual guess is that the nonrelativistic limit of the fundamental theory is the nonrelativistic Schrödinger equation for neutrons and protons interacting through two-body potentials. This is just an assumption; it may be that an adequate description of nuclei in which the meson degrees of freedom are suppressed is impossible. Also, even if taking the mesons into account by means of a nucleon–nucleon potential is justified, this potential is not necessarily a *two-body* potential. It may in addition contain nonnegligible three-body and four-body forces. Nevertheless, since there seems to be no good evidence against the assumption, the nonrelativistic Schrödinger equation with two-body forces is taken as a starting point for calculations on nuclei. Then we can try to answer the question: What properties does a realistic nucleon–nucleon potential imply for nuclei?

We have a good idea what the answer to this question should be—it should be the shell model. That is, one should find that nuclei can be accurately described in terms of an appropriate set of single-particle states and an effective interaction between the particles in these

* Work performed under the auspices of the U. S. Atomic Energy Commission.

¹ K. A. Brueckner, C. A. Levinson, and H. M. Mahmoud, *Phys. Rev.* **95**, 217 (1954).

² See also R. Rajaraman and H. A. Bethe, *Rev. Mod. Phys.* **39**, 745 (1967), following article.

states. So by starting from a realistic two-body force, we might hope to calculate the shell-model wave functions and the effective interaction.

This problem is too hard at the present time, and this is where nuclear matter enters the picture. It is a simplified problem whose solution is a first step towards the more difficult problem of the finite nucleus. Nuclear matter is a hypothetical system of equal numbers of neutrons and protons which fill all space at a uniform density. Of course, the Coulomb force is assumed to be turned off. The translational invariance of the system causes a tremendous simplification because it implies that the one-particle wave functions are plane waves.

Thus the most difficult part of a finite-nucleus calculation, the calculation of the single-particle wave functions, is absent from the nuclear-matter problem. The only problem is to calculate the energy of the system and the effective interaction between the particles.

The result of a nuclear-matter calculation is a value for \mathcal{E}/A , the energy per particle. This is to be calculated for each value of the particle density ρ , and one can therefore plot \mathcal{E}/A vs ρ . The saturation property of nuclear forces then implies that this curve should have a minimum value w_0 at some equilibrium density ρ_0 , as shown in Fig. 1.

The empirical values of w_0 and ρ_0 are deduced by extrapolating the observed properties of nuclei to infinite nuclear matter. The extrapolation of energy is carried out by means of the semiempirical mass formula, which expresses the energy of a nucleus with Z protons and N neutrons in the form

$$\mathcal{E} = a_1 A + a_2 A^{2/3} + a_3 Z^2 / A^{1/3} + a_4 (N - Z)^2 / 2A. \quad (1.1)$$

The first term is the volume term, the second term is the binding energy lost because of surface tension, the third term is the Coulomb energy, and the last term is the symmetry energy. For nuclear matter the last two terms vanish because we take $N = Z$ and neglect Coulomb forces. Furthermore, since A is very large for nuclear matter, the surface term is negligible compared to the volume term, and we therefore have $\mathcal{E} = a_1 A$. Thus w_0 is to be identified with a_1 , so that its empirical value^{3,4} is

$$w_0 = a_1 = -16 \text{ MeV}. \quad (1.2)$$

Similar ideas are used in the empirical determination of ρ_0 . For example, the interior density of a finite nucleus tends to be reduced by the Coulomb repulsion and increased by the surface tension, but both of these effects are absent in nuclear matter. These and other effects have been carefully considered by Brandow,⁵ who concludes that the equilibrium density of nuclear

matter is

$$\rho_0 = 0.170 \text{ F}^{-3}. \quad (1.3)$$

Other useful measures of the particle density are the interparticle spacing r_0 and the Fermi momentum k_F , which are defined by

$$1/\rho = (4\pi/3)r_0^3, \quad (1.4)$$

$$\rho = (2/3\pi^2)k_F^3. \quad (1.5)$$

The equilibrium values of these quantities are

$$r_0 = 1.12 \text{ F}, \quad (1.6)$$

$$k_F = 1.36 \text{ F}^{-1}. \quad (1.7)$$

In addition to being a first step towards a finite-nucleus calculation, the nuclear-matter problem has some intrinsic interest arising from the calculation of ρ_0 and a_1 . Nuclear matter calculations can also be helpful in deciding which realistic two-body force is the right one. Two potentials that give identical scattering phase shifts may give completely different results for nuclear matter, and a potential that implies unreasonable properties for nuclear matter can be discarded.

It should be clear from the last remark that the problem of devising a reliable method of calculation is distinct from the question of agreement between theory and experiment. A reliable method of calculation means an accurate solution of the many-body problem with an assumed two-body potential and provides an answer to the question: If the two-body potential were such and such, then what would be the equilibrium values of the density and energy per particle? The accuracy of the calculation is determined not by comparing the result with experiment but rather by estimating the magnitude of the higher-order terms that have been neglected. After a reliable method of calculation has been obtained, one can apply this method to see whether or not various nucleon-nucleon potentials give values of a_1 and ρ_0 that agree with the empirical values.

Only the Brueckner-Goldstone theory of nuclear matter will be treated in this paper. Brueckner invented this theory, Goldstone provided a formal basis for it, and most of the recent advances in physical understanding of the theory are due to Bethe and his collaborators.

There are other approaches to the theory of nuclear matter, which is, after all, simply the theory of an interacting Fermi gas at zero temperature. The Green's

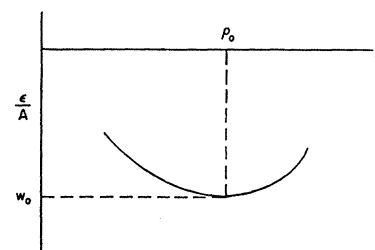


FIG. 1. Expected behavior of the energy per particle \mathcal{E}/A as a function of the particle density ρ for nuclear matter.

³ P. A. Seeger, Nucl. Phys. 25, 1 (1961).

⁴ A. E. S. Green, Phys. Rev. 95, 1006 (1954).

⁵ B. H. Brandow, Ph.D. thesis, Cornell University, 1964.

function method of statistical mechanics, invented by Martin and Schwinger, has been applied to nuclear matter by Puff.⁶ Lee and Yang's theory of quantum statistics has been developed by Mohling and applied by him to numerous problems, including nuclear matter.⁷ There is also Jastrow's method of correlated basis functions which is a variational method in which the trial wave function is taken to be a Slater determinant multiplied by a product of two-particle correlation functions, one correlation function for each pair of particles. This method has been developed⁸ by Feenberg, Clark, and others at Washington University, Saint Louis. Nothing will be said here about these theories except that *much* more work has been done with the Brueckner-Goldstone method than with any of the others. The Brueckner-Goldstone theory has been developed to a much higher degree than the others, and it appears that it can now be used to calculate accurately the properties of nuclear matter implied by a realistic nucleon-nucleon potential.

The Goldstone expansion, which is the starting point of the theory, is presented in Sec. II. The reaction matrix, which is necessary because of the strong short-range repulsion in the nucleon-nucleon potential, is introduced in Sec. III. Section IV is concerned with general properties of the reaction matrix, which is the fundamental quantity of the theory. The reference-spectrum method, which is a practical technique for calculating the reaction matrix, is explained in Sec. V. Section VI is a discussion of the related problems of convergence and the choice of the single-particle energy spectrum. Finally two short appendixes supplement the material of Secs. II and III.

II. THE GOLDSTONE EXPANSION

The Brueckner-Goldstone theory is based on the Goldstone expansion,⁹ which is a linked-cluster perturbation series for the ground-state energy of a many-body system. This formula will not be derived, but it will be described in a simple way, and how it is used in calculations will be made clear. What it amounts to is ordinary perturbation theory expressed in a form that is convenient for the many-body problem.

The Goldstone expansion works for any number of particles as long as the unperturbed ground state is nondegenerate. Thus it is valid for nuclear matter and for doubly magic finite nuclei. There is a similar formalism which works for nuclei with particles outside closed shells, but we will not need this.

Instead of specializing to nuclear matter immediately, therefore, we will first consider a system of a certain number A of identical nucleons whose Hamiltonian is the sum of the kinetic energies of all the particles

plus the sum of the two-body interactions between them, i.e.,

$$H = \sum_{i=1}^A T_i + \sum_{i<j}^A v_{ij} = H_0 + H_1. \quad (2.1)$$

The two-body potential v_{ij} corresponds to the realistic nucleon-nucleon force. It contains a strong short-range repulsion which is often approximated by an infinitely repulsive core of radius $c \approx 0.4$ F. Outside the core, the force is predominantly attractive, with a complicated dependence on spin, parity, and angular momentum. It approaches the one-pion-exchange potential at distances larger than 1.4 F.

Equation (2.1) splits H into two parts. The unperturbed Hamiltonian

$$H_0 = \sum_{i=1}^A (T_i + U_i) \quad (2.2a)$$

is the sum of the kinetic energy T and a one-body potential operator U . The perturbation

$$H_1 = \sum_{i<j}^A v_{ij} - \sum_{i=1}^A U_i \quad (2.2b)$$

is what is left over. The introduction of the single-particle potential U is intended to make numerical calculation easier. Since the total Hamiltonian does not involve U , the final result should in principle be independent of U . However, the energy is to be calculated as an expansion in powers of H_1 , and the expansion will converge more rapidly for some choices of U than for others. Thus we must try to choose U in such a way that the energy expansion converges rapidly enough to be useful for practical calculations. If we were doing an atomic problem, a good choice for U would be the self-consistent field obtained by solving the Hartree-Fock equations. The choice of U for nuclear matter will be discussed in Sec. VI.

The unperturbed problem is solved by finding the one-particle eigenfunctions ϕ_p of the operator $T+U$, which satisfy

$$(T_i + U_i)\phi_p(\mathbf{r}_i) = E_p\phi_p(\mathbf{r}_i). \quad (2.3)$$

The ϕ_p are assumed to form a complete orthonormal set of one-particle wave functions. The unperturbed ground state is represented by a Slater determinant Φ_0 formed by putting particles into the A one-particle states of lowest energy, i.e., by

$$\Phi_0 = (A!)^{-1/2} \mathcal{A}(\phi_1(\mathbf{r}_1) \cdots \phi_A(\mathbf{r}_A)). \quad (2.4)$$

The script \mathcal{A} is the antisymmetrizing operator, and Φ_0 is normalized to unity. It is this state which is assumed to be nondegenerate. Φ_0 is an eigenfunction of H_0 , and the eigenvalue ε_0 is the sum of the one-particle energies of the occupied states. Thus

$$H_0\Phi_0 = \varepsilon_0\Phi_0, \quad \varepsilon_0 = \sum_{n=1}^A E_n. \quad (2.5)$$

⁶ R. D. Puff, *Ann. Phys. (N.Y.)* **13**, 317 (1961).

⁷ F. Mohling, *Phys. Rev.* **124**, 583 (1961); **128**, 1365 (1962).

⁸ A recent and comprehensive discussion is given by J. W. Clark and P. Westhaus, *Phys. Rev.* **141**, 833 (1966).

⁹ J. Goldstone, *Proc. Roy. Soc. (London)* **A239**, 267 (1957).

The A one-particle states of lowest energy make up what is called the Fermi sea, and all states of higher energy are said to be above the Fermi sea.

The exact ground state ψ satisfies

$$H\psi = \varepsilon\psi, \tag{2.6}$$

and it is the eigenvalue ε that we want to calculate. Perturbation theory gives a formal expansion for ε , which, through third order in H_1 , is

$$\begin{aligned} \varepsilon = & \varepsilon_0 + \langle \Phi_0 | H_1 | \Phi_0 \rangle + \langle \Phi_0 | H_1 (\varepsilon_0 - H_0)^{-1} P H_1 | \Phi_0 \rangle \\ & + \langle \Phi_0 | H_1 (\varepsilon_0 - H_0)^{-1} P H_1 (\varepsilon_0 - H_0)^{-1} P H_1 | \Phi_0 \rangle \\ & - \langle \Phi_0 | H_1 | \Phi_0 \rangle \langle \Phi_0 | H_1 (\varepsilon_0 - H_0)^{-2} P H_1 | \Phi_0 \rangle \dots, \end{aligned} \tag{2.7}$$

$$P \equiv 1 - | \Phi_0 \rangle \langle \Phi_0 |. \tag{2.8}$$

The operator P projects off Φ_0 and ensures that Φ_0 does not occur as an intermediate state in any of the matrix elements.

The matrix elements in this formula involve many-body operators and many-body wave functions. In order to actually evaluate them, it is helpful to write the perturbation H_1 in the second quantized form

$$H_1 = \sum_{pqrs} \langle pq | v | rs \rangle a_p^\dagger a_q^\dagger a_s a_r - \sum_{pq} \langle p | U | q \rangle a_p^\dagger a_q, \tag{2.9}$$

$$\langle pq | v | rs \rangle \equiv \int \phi_p^*(\mathbf{r}_1) \phi_q^*(\mathbf{r}_2) v_{12} \phi_r(\mathbf{r}_1) \phi_s(\mathbf{r}_2) d\tau_1 d\tau_2, \tag{2.10}$$

$$\langle p | U | q \rangle \equiv \int \phi_p^*(\mathbf{r}_1) U_1 \phi_q(\mathbf{r}_1) d\tau_1, \tag{2.11}$$

$$a_r a_s + a_s a_r = 0, \quad a_r^\dagger a_s^\dagger + a_s^\dagger a_r^\dagger = 0, \quad a_r a_s^\dagger + a_s^\dagger a_r = \delta_{rs}. \tag{2.12}$$

The a 's are Fermion creation and destruction operators that satisfy the anticommutation relations (2.12); a_s destroys a particle in the one-particle state s and a_s^\dagger creates a particle in this state. From now on, the one-particle state ϕ_s will be referred to simply as the state s . The matrix elements are defined by Eqs. (2.10) and (2.11). The matrix element of v is calculated between pairs of two-particle wave functions, each of which is a simple product of one-particle functions; $\langle p | U | q \rangle$ is a matrix element of the one-particle potential U . Note that in the matrix element (2.10), p is associated with r in the sense that ϕ_p and ϕ_r have the same argument, and q is similarly associated with s . The summations in (2.9) run over all one-particle states, not over particles. It is clear that $\langle pq | v | rs \rangle = \langle qp | v | sr \rangle$, and it is understood that only one of these two identical terms is included in the sum. This is expressed by saying that the sum runs only over distinct matrix elements.

Now consider the second-order term in the perturbation series (2.7). We start with Φ_0 , apply H_1 to get a new state, divide by $(\varepsilon_0 - H_0)$, and apply H_1 again in order to get back to Φ_0 . Let us consider a single term in H_1 and see what it does to Φ_0 . We take the term $\langle ab | v | lm \rangle a_a^\dagger a_b^\dagger a_m a_l$, and we use the convention that indices a, b, c, \dots , at the beginning of the alphabet label states above the Fermi sea, while k, l, m, n, \dots , label states in the Fermi sea, and states p, q, r, s, \dots , could be either in the sea or above it.

What does $\langle ab | v | lm \rangle a_a^\dagger a_b^\dagger a_m a_l$ do to Φ_0 ? It destroys particles in states l and m in the Fermi sea and creates particles in states a and b above the Fermi sea. Thus it produces a new Slater determinant which differs from Φ_0 by having two vacancies in the Fermi sea and two occupied states above the Fermi sea. Vacancies in the Fermi sea are called holes, and occupied states above the Fermi sea are called particles. So Φ_0 is the Slater determinant with no particles and no holes, and any other Slater determinant can be specified by stating which particles and which holes are present. With this in mind we can represent the action of this operator on Φ_0 by means of the diagram shown in Fig. 2.

In the matrix element we work from right to left; in the diagrams, this corresponds to the upward direction. The interpretation of the diagram is that we started with the state Φ_0 with no particles and no holes (represented by the blank space below the diagram), then applied the operator $\langle ab | v | lm \rangle a_a^\dagger a_b^\dagger a_m a_l$ and obtained a new Slater determinant. This new Slater determinant has particles in a and b (represented by the upward directed lines) and it has holes in l and m (represented by the downward directed lines). This is an example of Rule 1 in Table I, the list of rules for diagrams.

The dashed line stands for the matrix element $\langle ab | v | lm \rangle$. Note that the lines labeled a and b (which are directed away from the vertex) appear on the left-hand side of the matrix element, while lines l and m (which are directed towards the vertex) appear on the right-hand side of the matrix element. This is in accord with Rule 2: The a^\dagger 's are associated with the left-hand side of the matrix element and always correspond to outgoing lines, and the a 's are associated with the right-hand side of the matrix element and always correspond to incoming lines. Also, a and l meet at the same end of the dashed line because the matrix element associates a with l , and similarly for m and b .

The new Slater determinant was obtained by applying one term of H_1 to Φ_0 . The next step is to operate on this new Slater determinant with $(\varepsilon_0 - H_0)^{-1}$. This

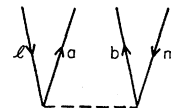


FIG. 2. Diagrammatic representation of $\langle ab | v | lm \rangle a_a^\dagger a_b^\dagger a_m a_l | \Phi_0 \rangle$.

clearly gives the reciprocal of the difference in energy between Φ_0 and the new state. Since the new Slater determinant has particles in states a and b above the Fermi sea and lacks particles in states l and m in the Fermi sea, we can write the reciprocal energy difference in the form $-(E_a + E_b - E_l - E_m)^{-1}$. This leads to Rule 3: The energy denominator for any intermediate state is equal to the sum of the particle energies minus the sum of the hole energies.¹⁰

We must next apply H_1 again and project onto Φ_0 . In this step we only need to consider those terms in H_1 that will carry the state $a_a^\dagger a_b^\dagger a_m a_l \Phi_0$ (which has two particles and two holes) back into Φ_0 . One such term is $\langle lm | v | ab \rangle a_l^\dagger a_m^\dagger a_b a_a$; this destroys particles a and b and fills up the holes l and m , thus taking us back to Φ_0 . We indicate this diagrammatically by terminating the upgoing and downgoing lines of Fig. 2 at a vertex to get the diagram of Fig. 3. All the holes and particles are destroyed, and we are left with the state Φ_0 , which has no holes and no particles. Note that Rule 2 is still obeyed; the outgoing lines at the upper vertex are l and m , and they appear on the left-hand side of the matrix element, while the incoming lines a and b are on the right-hand side of the matrix element.

The contribution of this diagram to the second-order term in the perturbation expansion is the product of three factors: the two-body matrix elements, the energy denominator, and the expectation value

$$\langle \Phi_0 | a_l^\dagger a_m^\dagger a_b a_a a_a^\dagger a_b^\dagger a_m a_l | \Phi_0 \rangle.$$

This expectation value is just ± 1 , depending on the exact order of the anticommuting Fermian operators.

TABLE I. Rules for diagrams.

(1)	An upward directed line represents an occupied state (particle) above the Fermi sea. A downward directed line represents an empty state (hole) in the Fermi sea.
(2)	The matrix element $\langle pq v rs \rangle$ is represented by a horizontal dashed line. At one end of the dashed line, r enters and p leaves; at the other end, s enters and q leaves. The final state $\langle pq $ is associated with the operator $a_p^\dagger a_q^\dagger$, which in turn corresponds to the outgoing lines. The initial state $ rs \rangle$ is associated with the operator $a_s a_r$, which in turn corresponds to the incoming lines.
(3)	The energy denominator is equal to the sum of the particle energies minus the sum of the hole energies.
(4)	The sign of the contribution of any diagram is given by $(-1)^{h+l+e+u}$, where h is the number of hole lines, l is the number of closed loops, e is the number of energy denominators, and u is the number of U interactions.

¹⁰ Every energy denominator is a negative quantity. However, it is most convenient to take the energy denominator to be positive, as is done in Rule 3. Then the minus sign is taken into account by the factor $(-1)^e$ of Rule 4.

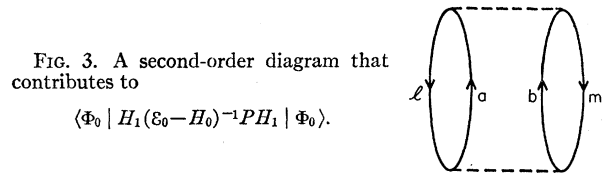


FIG. 3. A second-order diagram that contributes to

$$\langle \Phi_0 | H_1 (\mathcal{E}_0 - H_0)^{-1} P H_1 | \Phi_0 \rangle.$$

In the present case, the expectation value is $+1$, and the contribution of the diagram to \mathcal{E} is

$$-\frac{1}{2} \sum_{\substack{a, b > A \\ l, m \leq A}} \langle lm | v | ab \rangle (E_a + E_b - E_l - E_m)^{-1} \langle ab | v | lm \rangle, \quad (2.13)$$

where the minus sign arises from the energy denominator. Of course, a and b can be any states above the Fermi sea; so we must sum over all a and b above the Fermi sea and also over all l and m in the Fermi sea.

The factor $\frac{1}{2}$ comes from the restriction to distinct matrix elements in expression (2.9). That is, if we interchange l with m , and a with b , then *both* matrix elements in (2.13) are unchanged. Therefore, the summation in (2.13) includes each pair of distinct matrix elements twice, and the factor $\frac{1}{2}$ is needed in order to correct for this. Fortunately, no such correction factors are needed for the vast majority of diagrams. The small number of cases in which factors of $\frac{1}{2}$ occur will be pointed out when they arise.

There is a simple rule for telling whether the order of the Fermion operators gives a plus sign or a minus sign.⁹ The sign is just $(-1)^{h+l}$, where h is the number of hole lines and l is the number of closed loops. There is also a minus sign for each energy denominator,¹⁰ and there is a minus sign for each U interaction because of the negative sign of U in the perturbation Hamiltonian. These considerations lead to Rule 4 in the list of diagram rules. In Fig. 3, for example, we have $h=2$, $l=2$, $e=1$, $u=0$. This leads to the minus sign in expression (2.13).

We have calculated the contribution to the many-body matrix element $\langle \Phi_0 | H_1 (\mathcal{E}_0 - H_0)^{-1} P H_1 | \Phi_0 \rangle$ that arises from choosing one particular term of H_1 for the first H_1 interaction and another particular term of H_1 for the second H_1 interaction. There are many different possibilities for making these choices, and each possibility corresponds to a diagram. The many-body matrix element is a sum over all possibilities, and this is equivalent to a sum over all diagrams. Thus the diagrams are a device for keeping track of all the possible ways in which the sequence of operators

$$H_1 (\mathcal{E}_0 - H_0)^{-1} \cdots P H_1 (\mathcal{E}_0 - H_0)^{-1} P H_1$$

can lead from Φ_0 through a series of intermediate states and then back to Φ_0 again.

In the n th-order matrix element of this type, the initial eigenfunction is Φ_0 , then a particular term of H_1 leads to a new Slater determinant, then another term

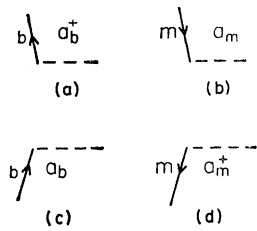


FIG. 4. Diagrammatic representation of the four different types of Fermion operator: (a) creation of a particle above the Fermi sea; (b) destruction of a particle in the Fermi sea, i.e., creation of a hole; (c) destruction of a particle above the Fermi sea; (d) creation of a particle in the Fermi sea, i.e., destruction of a hole.

of H_1 leads to another Slater determinant, etc. The diagrams will keep track of the change in the Slater determinant which is produced by each application of H_1 . The diagrams are all constructed from four fundamental pieces, each of which represents the effect of one of the four different kinds of Fermion operator illustrated in Fig. 4.

Further properties of the diagrams may be illustrated by considering another possibility for the second-order term in the energy. For the first H_1 we choose the term $\langle a | U | l \rangle a_a^\dagger a_l$. This creates a particle in state a and a hole in state l , and is represented diagrammatically by Fig. 5, where the cross at the end of the dashed line indicates a U interaction. Note that the outgoing line a appears on the left-hand side of the matrix element and the incoming line l appears on the right-hand side. The energy denominator is $(E_a - E_l)$. We must now choose a term from H_1 which will return the system to Φ_0 . Let us choose the term $\langle lm | v | am \rangle a_l^\dagger a_m^\dagger a_m a_a$, which is represented diagrammatically by the upper interaction of Fig. 6. The destruction of particle a and the filling of the hole l are shown at the left-hand end of the upper dashed line. At the right-hand end of this dashed line, the $a_m^\dagger a_m$ part of the operator destroys a particle in state m in the Fermi sea and then creates it right back again. As shown in Fig. 4, the operator a_m^\dagger produces an outgoing hole line, and a_m produces an incoming hole line. Since the net result is to leave the Slater determinant unchanged, we join these two hole lines together to make a bubble. Thus Fig. 6 is another second-order diagram that contributes to the energy. Its contribution is the product of the matrix elements and the energy denominator, summed over all states a above the Fermi sea and all l and m in the Fermi sea. What does the sign rule give for the diagram? Since $h=2, l=2, e=1, u=1$, the contribution to \mathcal{E} has a positive sign¹¹ and its value is

$$\sum_{\substack{a>A \\ l,m \leq A}} \langle lm | v | am \rangle (E_a - E_l)^{-1} \langle a | U | l \rangle. \quad (2.14)$$

Now consider the first of the two third-order terms in

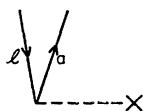


FIG. 5. Diagrammatic representation of $\langle a | U | l \rangle a_a^\dagger a_l | \Phi_0 \rangle$.

¹¹ For the purpose of the sign rule, a bubble (such as the one at the top of Fig. 6) contributes one hole line and one closed loop.

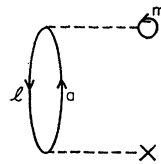


FIG. 6. A second-order diagram that contributes to $\langle \Phi_0 | H_1 (\epsilon_0 - H_0)^{-1} P H_1 | \Phi_0 \rangle$.

expression (2.7) for the energy. Several diagrams that contribute to this matrix element are shown in Fig. 7. As an example, the contribution to \mathcal{E} from diagram 7(e) is given by

$$+ \sum_{\substack{a,b,c>A \\ l,m,n \leq A}} \frac{\langle ln | v | ca \rangle \langle cm | v | bn \rangle \langle ab | v | lm \rangle}{(E_c + E_a - E_l - E_n)(E_a + E_b - E_l - E_m)}. \quad (2.15)$$

The plus sign in this formula follows from the fact that $h+l+e+u=3+1+2+0=6$. There are many more third-order diagrams, and they can all be evaluated by the methods that have been described. The basic rules for diagrams are summarized in Table I.

The perturbation series (2.7) gets more complicated in third order. There are two terms instead of one, and a new feature appears in the diagrams. Among the diagrams that contribute to the first of the two third-order matrix elements in expression (2.7) is the one shown in Fig. 8. This is a perfectly legitimate diagram. The first H_1 creates two particles and two holes, and the second H_1 destroys particle n in the Fermi sea and creates it right back again, and the same for k . Then the last H_1 takes the system back to Φ_0 .

This diagram is disconnected, and that such diagrams should appear is a catastrophe. The reason is that, in the limit of a large number of particles, the contribution of a connected diagram is proportional to the number of particles, and the contribution of a diagram that consists of two disjoint pieces is proportional to the square of the number of particles.^{12,13} So in third order a term arises that is proportional to the square of the number of particles. This is nonsense because the energy of a very large system must be proportional to the number of particles. The solution to the difficulty lies in the second third-order term in formula (2.7). One can show that this second term exactly cancels all the disconnected diagrams that contribute to the first term, and thereby leaves only connected diagrams for the third-order contribution. One can demonstrate the same cancellation in fourth order,

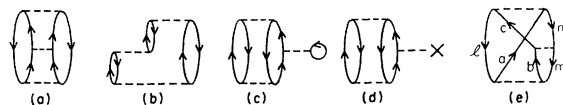


FIG. 7. Several of the third-order diagrams that contribute to $\langle \Phi_0 | H_1 (\epsilon_0 - H_0)^{-1} P H_1 (\epsilon_0 - H_0)^{-1} P H_1 | \Phi_0 \rangle$.

¹² N. M. Hugenholtz, *Physica* **23**, 481 (1957).

¹³ B. H. Brandow, *Rev. Mod. Phys.* **39**, 771 (1967), see Appendix C.

fifth order, etc., but the amount of work required increases at a tremendous rate. Goldstone's achievement was to show that this cancellation is exact in every order of perturbation theory; in other words the n th-order contribution to the energy is just the sum of all connected n th-order diagrams. This fact leads to the Goldstone expansion,⁹ which can be stated in the form¹⁴

Goldstone expansion:

$$\varepsilon = \varepsilon_0 + \text{sum of all connected diagrams.} \quad (2.16)$$

Thus the Goldstone expansion accomplishes two things. First, it solves a problem that arises in all many-body theories—the problem of isolating the correct dependence of physical quantities on the particle number. The exact ground-state energy is now exhibited as a sum of terms, each of which is proportional to the number of particles. Secondly, the Goldstone expansion gives a simple and explicit prescription for calculating every order of perturbation theory. This is important because certain classes of diagrams have to be summed to infinite order before the expansion can be used for nuclear matter.

Let us now write out the Goldstone result explicitly to first order. We must evaluate all the first-order diagrams and add their contributions to ε_0 . The three first-order diagrams are shown in Fig. 9. The first diagram comes from applying the term

$$\langle mn | v | mn \rangle a_m^\dagger a_n^\dagger a_n a_m$$

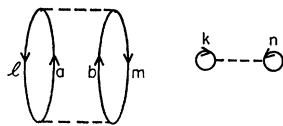
from the perturbation Hamiltonian to the unperturbed ground state Φ_0 and projecting the result back onto Φ_0 . The second diagram is the exchange of the first. And the third diagram involves the one-particle potential U . The contributions of the diagrams to the energy are, respectively,

$$\begin{aligned} \frac{1}{2} \sum_{m,n \leq A} \langle mn | v | mn \rangle, & \quad -\frac{1}{2} \sum_{m,n \leq A} \langle mn | v | nm \rangle, \\ & \quad - \sum_{n \leq A} \langle n | U | n \rangle. \end{aligned} \quad (2.17)$$

The factor $\frac{1}{2}$ in the first two terms arises from the restriction to distinct matrix elements in expression (2.9) for H_1 . Since $\langle mn | v | mn \rangle = \langle nm | v | nm \rangle$, summing over all m and n counts each distinct matrix element twice, and the factor $\frac{1}{2}$ corrects for this double counting. The physical reason for the $\frac{1}{2}$ is quite clear: in summing up the interactions of pairs of particles, each pair must be counted only once.

FIG. 8. A disconnected third-order diagram that contributes to

$$\begin{aligned} & \langle \Phi_0 | H_1 (\varepsilon_0 - H_0)^{-1} \\ & \times P H_1 (\varepsilon_0 - H_0)^{-1} P H_1 | \Phi_0 \rangle. \end{aligned}$$



¹⁴ The treatment of the exclusion principle in intermediate states, which has not yet been specified, is discussed in Appendix A.

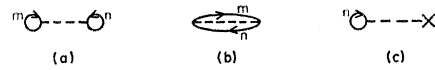


FIG. 9. The first-order Goldstone diagrams. The sum of their contributions is $\langle \Phi_0 | H_1 | \Phi_0 \rangle$, the first-order term in the energy.

To the sum of the first-order diagrams we must add the unperturbed energy ε_0 ,

$$\varepsilon_0 = \sum_{n \leq A} E_n = \sum_{n \leq A} \langle n | T + U | n \rangle, \quad (2.18)$$

which is just the sum of the energies of the occupied states. Note that the terms involving U in expressions (2.17) and (2.18) cancel out. This cancellation is automatic and does not depend on a particular choice for U . Thus, to first order, the formula for the ground-state energy is

$$\begin{aligned} \varepsilon = & \sum_{n \leq A} \langle n | T | n \rangle \\ & + \frac{1}{2} \sum_{m,n \leq A} (\langle mn | v | mn \rangle - \langle mn | v | nm \rangle). \end{aligned} \quad (2.19)$$

This expression still depends on U because the one-particle wave functions, which are used in the calculation of the matrix elements, depend on U .

III. THE REACTION MATRIX AND THE BRUECKNER-GOLDSTONE EXPANSION

The Goldstone expansion cannot be used in its present form for nuclear calculations because the strong short-range repulsion in the nucleon-nucleon potential makes all the matrix elements very large, and the series cannot converge. The next step is to introduce Brueckner's reaction matrix and convert the expansion to one in which the potential is eliminated in favor of the reaction matrix.⁹ Since the reaction matrix is well-behaved even for a singular two-body force, all terms in this new perturbation series—the Brueckner-Goldstone expansion—are finite and of reasonable size.

The strong short-range repulsion causes a similar difficulty in the problem of nucleon-nucleon scattering. If one calculates the scattering amplitude to first order in v , that is, if one uses the Born approximation, then one obtains a large and inaccurate result. But if one calculates to all orders in v , which amounts to solving the two-particle Schrödinger equation, then one obtains the correct result.

The procedure followed for nuclei is analogous to the treatment of nucleon-nucleon scattering. The diagrams in the Goldstone expansion are rearranged in such a way that each matrix element of v is replaced by an infinite series which takes account of the two-body interaction to all orders of the potential. The quantity that replaces the two-body potential is called the reaction matrix; and calculating the reaction matrix is equivalent to solving a Schrödinger equation which describes the scattering of two particles in the presence of all the others.

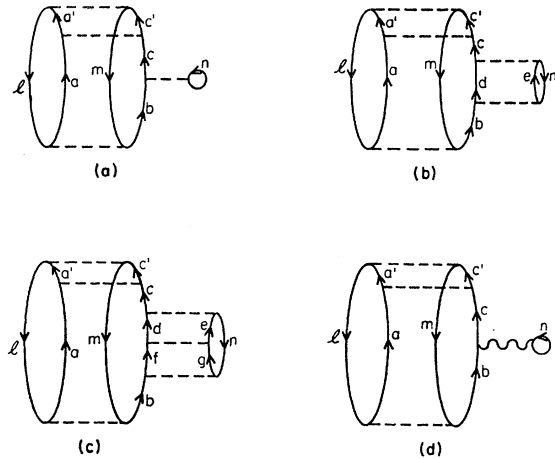


FIG. 10. Diagrams illustrating the summation of ladder diagrams to obtain the G matrix. Diagrams 10(a), (b), (c) are the first three members of an infinite sequence of ladder diagrams whose sum is diagram 10(d), in which the wiggly line represents the G matrix.

We illustrate the method by applying it to the diagram shown in Fig. 10(a). Let us concentrate our attention on the v interaction with the bubble at one end. The outgoing lines are c and n , and the incoming lines are b and n ; so the matrix element is $\langle cn | v | bn \rangle$. This gives the bubble interaction to first order in v . To this diagram we now add an entire infinite sequence of diagrams, each of which is exactly the same as the original diagram except that this first-order v interaction is replaced by a ladder containing two or more v interactions. Figures 10(b) and 10(c) show the next two diagrams in this sequence, and the rest are constructed by putting in more dashed lines between the two up-going lines.

The contribution of the first diagram contains the factor $\langle cn | v | bn \rangle$, and the contribution of any other diagram in the sequence is exactly the same except that this matrix element is replaced by a more complicated expression. The appropriate expressions for diagrams 10(a), (b), (c) are given, respectively, by

$$\langle cn | v | bn \rangle, \tag{3.1}$$

$$- \sum_{d,e>A} \langle cn | v | de \rangle (E_d + E_e - W)^{-1} \langle de | v | bn \rangle, \tag{3.2}$$

$$+ \sum_{d,e,f,g>A} \langle cn | v | de \rangle (E_d + E_e - W)^{-1} \langle de | v | fg \rangle (E_f + E_g - W)^{-1} \langle fg | v | bn \rangle, \tag{3.3}$$

where

$$W = E_l + E_m + E_n - E_a. \tag{3.4}$$

In the second diagram, for example, there are two matrix elements with an energy denominator in between, instead of the single matrix element $\langle cn | v | bn \rangle$. In the upper interaction, the outgoing lines are c and n , and the incoming lines are d and e .

Then there is an energy denominator, which will be discussed in a moment. And in the lower interaction the outgoing lines are d and e and the incoming lines are b and n . Lines d and e can represent any states above the Fermi sea; so we must sum over d and e .

The energy denominator for the second diagram, at the level of lines d and e , is the sum of the particle energies minus the sum of the hole energies and is therefore equal to $E_a + E_d + E_e - E_l - E_m - E_n$. It is convenient to write this in the form $E_d + E_e - W$, where W is called the starting energy and is given by Eq. (3.4).

The second diagram has the same number of hole lines, the same number of closed loops, and the same number of U interactions as the first, but it has one more energy denominator. Thus it gets a minus sign relative to the first diagram, as indicated in expression (3.2).

The contribution from the third-order ladder of Fig. 10(c) is obtained by similar reasoning and is given by (3.3). It is obtained by starting at the top with $\langle cn | v | de \rangle$, then going from d and e to two other states f and g above the Fermi sea, and then finally returning to b and n . Note that the rest of the diagram is not allowed to have any interaction between the first and last interactions in the ladder. Therefore, the starting energy W , which depends on the rest of the diagram, remains constant while the contributions from the ladders are being summed.

The sum of the contributions from this infinite sequence of ladders defines an element of the reaction matrix, which we call G . In the diagrams, a matrix element of G is indicated by a wiggly line as shown in Fig. 10(d). Thus the sum of the sequence of ladder diagrams of Fig. 10 is a single diagram 10(d) which looks exactly like the original diagram 10(a) except that the v -matrix bubble has become a G matrix. Note that G depends on the starting energy W , and that in any ladder all the interactions (except possibly the first and last) are dashed lines drawn between two upgoing lines.

It is convenient to define the two-particle operators Q and e by the equations

$$Q | pq \rangle = \begin{cases} | pq \rangle & \text{if } p > A \text{ and } q > A, \\ 0 & \text{otherwise,} \end{cases} \tag{3.5}$$

$$e | pq \rangle = (E_p + E_q - W) | pq \rangle, \tag{3.6}$$

in which $| pq \rangle$ stands for $\phi_p(\mathbf{r}_1)\phi_q(\mathbf{r}_2)$. The Pauli operator Q annihilates a two-particle state unless both particles are above the Fermi sea, and e gives the energy of the two-particle state minus the starting energy.

By using these operators, we can write the two-particle operator G in the form

$$G(W) = v - v(Q/e)v + v(Q/e)v(Q/e)v - + \dots \tag{3.7}$$

Actually, this is the definition of G ; in our treatment of Fig. 10(a) we simply noticed that the sum of ladder contributions agrees with this definition. For example, in the expression (3.2) representing the second-order ladder, the effect of Q is to restrict the summation to states d and e above the Fermi sea, and e operating on the two-particle state $|de\rangle$ just gives the energy denominator $(E_e + E_d - W)$.

The expansion (3.7) is equivalent to the integral equation

$$G(W) = v - v(Q/e)G(W). \quad (3.8)$$

For a given starting energy W , G is a well-defined Hermitian two-particle operator. It is Hermitian because Q , e , and v are all Hermitian, and therefore every term in the expansion (3.7) is Hermitian.

Summing the appropriate sequence of ladder diagrams has led to a single diagram in which one of the

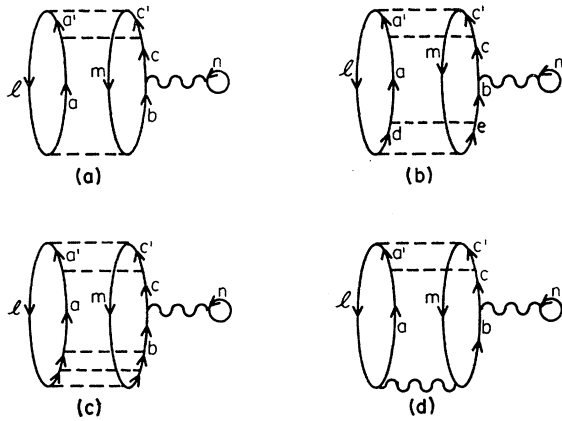


FIG. 11. Conversion from a v interaction to a G matrix. Diagrams 11(a), (b), (c) are the first three ladder diagrams in the sequence which converts the lowest v interaction of diagram 11(a) to a G matrix, as shown in diagram 11(d).

v interactions is replaced by the reaction matrix. This is very desirable because the matrix elements of G turn out to be well-behaved even when the strong short-range repulsion causes the matrix elements of v to become very large or infinite. The next step is to convert the rest of the v interactions in diagram 10(d) into G matrices by the same method.

The first three diagrams in the sequence that converts the lowest v to a G are shown in Fig. 11(a), (b), (c). The first two ladder contributions, which arise from 11(a) and 11(b), are

$$\langle ab | v | lm \rangle, \quad (3.9)$$

$$- \sum_{a, e > A} \langle ab | v | de \rangle (E_d + E_e - W)^{-1} \langle de | v | lm \rangle = \langle ab | -v(Q/e)v | lm \rangle, \quad (3.10)$$

where

$$W = E_l + E_m. \quad (3.11)$$

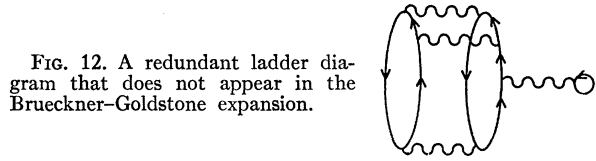


FIG. 12. A redundant ladder diagram that does not appear in the Brueckner-Goldstone expansion.

The criterion for choosing the correct sequence of ladder diagrams is that the contribution from the n th-order ladder must reproduce the matrix element of the n th term in the expansion (3.7). For example, since the contribution of the second-order ladder is clearly equal to $\langle ab | -v(Q/e)v | lm \rangle$, the second diagram in Fig. 11 is the correct one. Note that the starting energy W is equal to $E_l + E_m$, which is just the energy of the initial two-particle state in the matrix element. When the starting energy is equal either to the energy of the initial two-particle state or to the energy of the final two-particle state, we say that the G -matrix is calculated on the energy shell. In all other cases, G is said to be calculated off the energy shell. Therefore, the G matrix that replaces the lowest v interaction is on the energy shell, but the G matrix corresponding to the bubble interaction is off the energy shell.

Summing the sequence of Fig. 11(a), (b), (c), ... yields Fig. 11(d), in which the bottom v interaction is replaced by a G matrix. If now the same treatment were applied to each of the last two v interactions, the result would be the diagram given in Fig. 12. But this would be wrong. For, a typical ladder diagram of the type included in this G -matrix diagram is as shown in Fig. 13. The latter could be a first-order ladder in the top G matrix of Fig. 12 and a second-order ladder in the next G matrix, or it could be a second-order ladder in the top G matrix and first-order ladder in the next G matrix. Therefore, Fig. 13 is included *twice* in the G -matrix diagram of Fig. 12.

We should have noticed that Fig. 11(d) is the second-order ladder diagram in the series whose sum is the G -matrix diagram of Fig. 14. In this last diagram, all ladder diagrams of type 11(d) are counted exactly once. Thus the diagram of Fig. 12 is completely unnecessary; it is redundant and should simply be omitted.

By summation of the appropriate sequences of ladder diagrams, the original v -matrix diagram 10(a) has been transformed into the diagram of Fig. 14, which contains only G matrices. The same methods can be applied to *any* v -matrix diagram. Starting with an arbitrary v -matrix diagram, one successively converts each v to a G by summing the proper sequence of ladder

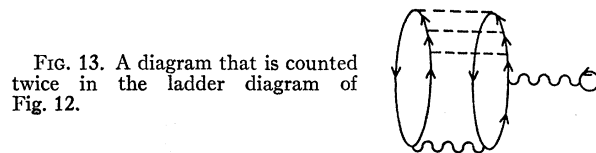


FIG. 13. A diagram that is counted twice in the ladder diagram of Fig. 12.

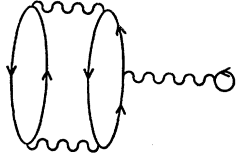


FIG. 14. The G -matrix diagram that is obtained from the v -matrix diagram of Fig. 10(a) by appropriate summation of ladders.

diagrams. In this way, one obtains an expansion in which v is entirely eliminated in favor of G . (Additional details are given in Appendix B.)

The resulting expansion is called the Brueckner–Goldstone expansion. It tells us simply to replace v by G in the Goldstone expansion, and to omit ladder diagrams such as Fig. 12 in order to avoid double counting. In this new expansion, every term is finite and well-behaved, even when the potential contains a strong short-range repulsion. The Brueckner–Goldstone expansion is the starting point for nuclear calculations.

IV. PROPERTIES OF THE REACTION MATRIX

The basic quantity in the Brueckner–Goldstone expansion is the G matrix. We must therefore learn what its properties are and how to calculate it. G always operates on a two-particle wave function Φ_{rs} which is just a product of one-particle functions; i.e., on

$$\Phi_{rs}(\mathbf{r}_1, \mathbf{r}_2) \equiv \phi_r(\mathbf{r}_1)\phi_s(\mathbf{r}_2) \equiv |rs\rangle. \quad (4.1)$$

This is called the *unperturbed* two-body wave function, and it is useful to define a *correlated* two-body wave function Ψ_{rs} by the equation

$$\Psi_{rs} = \Phi_{rs} - (Q/e)G\Phi_{rs}. \quad (4.2)$$

It then follows that

$$v\Psi_{rs} = [v - v(Q/e)G]\Phi_{rs} = G\Phi_{rs}, \quad (4.3)$$

and substituting $G\Phi_{rs} = v\Psi_{rs}$ into Eq. (4.2) shows that the correlated two-particle wave function satisfies

$$\Psi_{rs} = \Phi_{rs} - (Q/e)v\Psi_{rs}. \quad (4.4)$$

G is always calculated by first calculating the wave function Ψ_{rs} . The connection between this wave function and the wave function for nucleon–nucleon scattering will be established later on in this section.

Up to this point everything has been valid for any number of particles. From now on, however, we will specialize to infinite nuclear matter. So before continuing the study of the G matrix, it is useful to take note of a number of relevant facts about nuclear matter.

It is assumed from the beginning that the system of nuclear matter is homogeneous and isotropic. This implies that the single-particle wave functions are plane waves represented by

$$\phi_s(\mathbf{r}_1) = \Omega^{-1/2} \exp(i\mathbf{k}_s \cdot \mathbf{r}_1). \quad (4.5)$$

The nucleons are assumed to be contained in a very large box of volume Ω , and the wave vectors \mathbf{k} satisfy periodic boundary conditions. In the unperturbed

ground state, all states with momentum less than the Fermi momentum k_F are occupied and all others are empty. All summations over one-particle states are replaced by integrals in the usual way. That is,

$$\sum_s \rightarrow 4 \frac{\Omega}{(2\pi)^3} \int d^3k_s. \quad (4.6)$$

The factor 4 arises from spin–isospin degeneracy, which implies that every spatial wave function can accommodate four nucleons. As an example, the particle density ρ in nuclear matter is

$$\begin{aligned} \rho(\mathbf{r}) &= \sum_{m \leq A} |\phi_m(\mathbf{r})|^2 \rightarrow 4 \frac{\Omega}{(2\pi)^3} \int_{k_m < k_F} d^3k_m \Omega^{-1} \\ &= (2/3\pi^2) k_F^3. \end{aligned} \quad (4.7)$$

The density is proportional to the volume of the Fermi sphere and is independent of position.

In a similar way one finds that the average kinetic energy of a particle in the Fermi sea is

$$\bar{T} = \frac{3}{10} k_F^2. \quad (4.8)$$

Here, and in the rest of this paper, we use units such that \hbar^2/M is unity, where M is the nucleon mass. Then the dimensions of energy are those of k_F^2 , which is the square of an inverse length, and the conversion factor is $1 F^{-2} = 41.5 \text{ MeV}$. The equilibrium value of k_F for nuclear matter is⁵ $1.36 F^{-1}$, and this gives an average kinetic energy of 23 MeV.

The one-particle kinetic energy operator T is clearly diagonal in the plane-wave representation, and therefore the one-particle potential U is also diagonal in this representation. This is because the plane waves must be eigenfunctions of $(T+U)$. Therefore the one-particle potential operator is completely specified by giving its diagonal matrix element as a function of momentum. If we call this matrix element $U(k)$, then the energy of a plane wave state of momentum k is

$$E(k) = T(k) + U(k). \quad (4.9)$$

The kinetic energy is equal to $\frac{1}{2}k^2$, and $U(k)$ is chosen to depend only on the magnitude of the vector \mathbf{k} , not on its direction.

Since the one-particle potential is diagonal in momentum space, the many-body operator

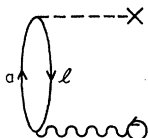
$$\sum_i U_i$$

cannot change the momentum of a many-body state. The same is true of

$$\sum_{i < j} v_{ij}$$

for any physically reasonable nucleon–nucleon potential, and the perturbation Hamiltonian H_1 therefore conserves momentum. Thus every Slater determinant that occurs in the perturbation expansion must have the same total momentum as the filled Fermi sea, and

FIG. 15. A diagram that does not contribute to the energy of nuclear matter because of momentum conservation.



this momentum is zero. This fact has important consequences for the diagrams.

For example, the diagram shown in Fig. 15 has an intermediate state whose momentum is $\mathbf{k}_a - \mathbf{k}_l$. This cannot be zero because $k_a > k_F$ and $k_l < k_F$; hence this diagram cannot contribute to the energy of nuclear matter. The top and bottom matrix elements both vanish because each one changes the total momentum. Thus there are many diagrams that never need to be considered for the case of nuclear matter because they violate the requirement of momentum conservation.

This requirement makes possible the enumeration of the low-order diagrams for nuclear matter. The first-order diagrams are shown in Fig. 16. They are the same as those of Fig. 9 except that the v interactions are replaced by G matrices. The first-order approximation for the energy is obtained from the Goldstone result, formula (2.19), when v is replaced by G .

Momentum conservation causes most of the second-order diagrams to vanish. A diagram that conserves momentum is shown in Fig. 17, but this is a ladder diagram and all v -matrix diagrams represented by it are included in the first-order diagram 16(a); so Fig. 17 must be omitted. The result is that there are no second-order diagrams at all.

There are, however, several third-order diagrams, some of which are shown in Fig. 18. There are 16 other third-order diagrams, but each one can be considered an exchange diagram of one of those already shown.

What diagrams does one actually evaluate in practice? In a detailed nuclear matter calculation, one evaluates only the first-order G -matrix diagrams. (The first-order U diagram cancels out as explained at the end of Sec. II.) The effect of certain higher-order diagrams is taken into account by the proper choice of U . There is good reason to believe that the result obtained in this way is correct to within 1-2 MeV per particle. The proper choice of U will be discussed after our study of the G matrix, to which we now return.

The fact that the one-particle wave functions are plane waves means that the two-particle wave function has only a trivial dependence on the center-of-mass coordinate of the two interacting particles. This trivial dependence on the center-of-mass coordinate must be separated from the physically interesting dependence on the relative position vector. We must also investigate

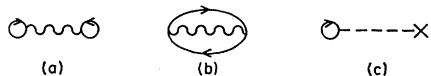
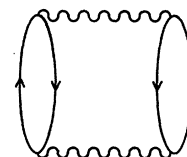


FIG. 16. The first-order diagrams of the Brueckner-Goldstone expansion.

FIG. 17. A second-order diagram in which momentum is conserved, but which is redundant and therefore does not appear in the Brueckner-Goldstone expansion.



the volume dependence of the G matrix and of the two-body wave function.

The unperturbed two-particle wave function in nuclear matter is

$$\begin{aligned} \Phi_{rs}(\mathbf{r}_1, \mathbf{r}_2) &= \Omega^{-1} \exp(i\mathbf{k}_r \cdot \mathbf{r}_1) \exp(i\mathbf{k}_s \cdot \mathbf{r}_2) \\ &= \Omega^{-1} \exp(i\mathbf{K}_{rs} \cdot \mathbf{R}) \exp(i\mathbf{k}_{rs} \cdot \mathbf{r}), \end{aligned} \quad (4.10)$$

where

$$\begin{aligned} \mathbf{R} &= \frac{1}{2}(\mathbf{r}_1 + \mathbf{r}_2), & \mathbf{K}_{rs} &= \mathbf{k}_r + \mathbf{k}_s, & \mathbf{k}_r &= \frac{1}{2}\mathbf{K}_{rs} + \mathbf{k}_{rs}, \\ \mathbf{r} &= \mathbf{r}_1 - \mathbf{r}_2, & \mathbf{k}_{rs} &= \frac{1}{2}(\mathbf{k}_r - \mathbf{k}_s), & \mathbf{k}_s &= \frac{1}{2}\mathbf{K}_{rs} - \mathbf{k}_{rs}. \end{aligned} \quad (4.11)$$

Here \mathbf{R} is the center-of-mass coordinate of the two interacting particles, \mathbf{r} is their relative position vector, \mathbf{K}_{rs} is the total momentum, and \mathbf{k}_{rs} is the relative momentum. The factor $\frac{1}{2}$ in the formula for \mathbf{k}_{rs} occurs because the reduced mass for two nucleons is half the actual nucleon mass. Equation (4.11) also contains formulas for the individual momentum vectors \mathbf{k}_r and \mathbf{k}_s in terms of the total and relative momenta. Equation (4.10) explicitly isolates the dependence of Φ_{rs} on Ω and on \mathbf{R} .

In terms of total and relative momenta, the operators e and Q are given by

$$\begin{aligned} e |pq\rangle &= [E(\frac{1}{2}\mathbf{K}_{pq} + \mathbf{k}_{pq}) + E(\frac{1}{2}\mathbf{K}_{pq} - \mathbf{k}_{pq}) - W] |pq\rangle \\ &\equiv e(\mathbf{k}_{pq}, \mathbf{K}_{pq}) |pq\rangle, \end{aligned} \quad (4.12)$$

$$\begin{aligned} Q |pq\rangle &= \begin{cases} |pq\rangle & \text{if } \left\{ \begin{array}{l} |\frac{1}{2}\mathbf{K}_{pq} + \mathbf{k}_{pq}| > k_F \\ |\frac{1}{2}\mathbf{K}_{pq} - \mathbf{k}_{pq}| > k_F \end{array} \right\} \\ 0 & \text{otherwise} \end{cases} \\ &\equiv Q(\mathbf{k}_{pq}, \mathbf{K}_{pq}) |pq\rangle. \end{aligned} \quad (4.13)$$

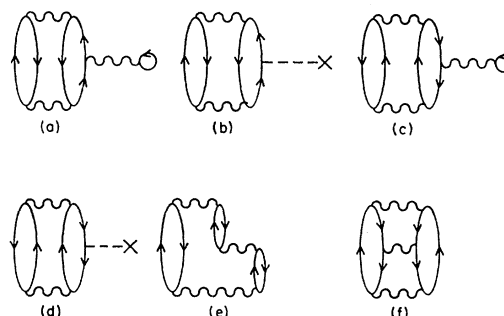


FIG. 18. Some third-order diagrams that contribute to the energy of nuclear matter. All other third-order diagrams are generated by forming exchange diagrams from the ones shown here.

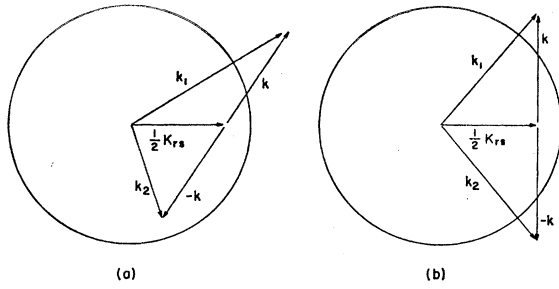


FIG. 19. Two-particle intermediate states in momentum space, as determined by the variable relative momentum \mathbf{k} and the fixed total momentum \mathbf{K}_{rs} . In 19(a), \mathbf{k}_1 lies outside the sphere of radius k_F , and \mathbf{k}_2 lies inside this sphere; hence particle 1 is above the Fermi sea while particle 2 is in the sea. In 19(b), both particles are above the sea.

Formulas (4.12) and (4.13) also serve to define $e(\mathbf{k}, \mathbf{K})$ and $Q(\mathbf{k}, \mathbf{K})$, which are simply numerical functions of (\mathbf{k}, \mathbf{K}) .

The operators Q , e , and v all conserve the total momentum of a two-particle state. Hence the total momentum of the correlated wave function Ψ_{rs} will be equal to the total momentum of the unperturbed two-particle wave function. Therefore the dependence of Ψ_{rs} on \mathbf{R} and on Ω will be the same as that of Φ_{rs} , and we can write

$$\Psi_{rs} = \Omega^{-1} \exp(i\mathbf{K}_{rs} \cdot \mathbf{R}) \psi_{rs}(\mathbf{r}). \quad (4.14)$$

All the two-body correlations are contained in the function $\psi_{rs}(\mathbf{r})$, which is independent of Ω and depends only on the relative position vector.

We can now write a useful formula for the G matrix. Since $G\Phi_{rs} = v\Psi_{rs}$, we have

$$\begin{aligned} \langle pq | G | rs \rangle &= \int \Phi_{pq}^* v \Psi_{rs} d^3r_1 d^3r_2, \\ &= \int \Omega^{-1} \exp(-i\mathbf{K}_{pq} \cdot \mathbf{R}) \exp(-i\mathbf{k}_{pq} \cdot \mathbf{r}) \\ &\quad \times v(\mathbf{r}) \Omega^{-1} \exp(i\mathbf{K}_{rs} \cdot \mathbf{R}) \psi_{rs}(\mathbf{r}) d^3r d^3R. \end{aligned} \quad (4.15)$$

The integration over \mathbf{R} gives the product of the volume Ω and a Kronecker delta function of total momentum. The result is

$$\langle pq | G | rs \rangle = \Omega^{-1} \delta(\mathbf{K}_{pq}, \mathbf{K}_{rs}) \langle \mathbf{k}_{pq} | G | \mathbf{k}_{rs} \rangle, \quad (4.16)$$

where

$$\langle \mathbf{k}_{pq} | G | \mathbf{k}_{rs} \rangle = \int \exp(-i\mathbf{k}_{pq} \cdot \mathbf{r}) v(\mathbf{r}) \psi_{rs}(\mathbf{r}) d^3r. \quad (4.17)$$

The matrix element $\langle \mathbf{k}_{pq} | G | \mathbf{k}_{rs} \rangle$ is independent of the volume and is what is usually called the G matrix. Of course, it depends on the total momentum and on the starting energy. To obtain the "real" G matrix, however, it is necessary to divide this quantity by the volume. The "real" G matrix has dimensions of energy, i.e., the square of an inverse length; hence $\langle \mathbf{k}_{pq} | G | \mathbf{k}_{rs} \rangle$

is dimensionally a length. A typical value of the diagonal element representing the interaction of two particles in the Fermi sea is $-10 F \approx -400 \text{ MeV} \cdot F^3$.

In terms of relative and center-of-mass coordinates, Eq. (4.4) for the correlated wave function becomes

$$\begin{aligned} \exp(i\mathbf{K}_{rs} \cdot \mathbf{R}) \psi_{rs}(\mathbf{r}) &= \exp(i\mathbf{K}_{rs} \cdot \mathbf{R}) \exp(i\mathbf{k}_{rs} \cdot \mathbf{r}) \\ &\quad - (Q/e)v \exp(i\mathbf{K}_{rs} \cdot \mathbf{R}) \psi_{rs}(\mathbf{r}). \end{aligned} \quad (4.18)$$

The last term can be written

$$\begin{aligned} &\sum_{\mathbf{k}, \mathbf{K}} (Q/e) |\mathbf{k}\mathbf{K}\rangle \langle \mathbf{k}\mathbf{K} | v \exp(i\mathbf{K}_{rs} \cdot \mathbf{R}) \psi_{rs}(\mathbf{r}) \\ &= \sum_{\mathbf{k}, \mathbf{K}} \frac{Q(\mathbf{k}, \mathbf{K})}{e(\mathbf{k}, \mathbf{K})} \frac{\exp(i\mathbf{K} \cdot \mathbf{R}) \exp(i\mathbf{k} \cdot \mathbf{r})}{\Omega} \\ &\quad \times \int \frac{\exp(-i\mathbf{K} \cdot \mathbf{R}') \exp(-i\mathbf{k} \cdot \mathbf{r}')}{\Omega} \\ &\quad \times v(\mathbf{r}') \exp(i\mathbf{K}_{rs} \cdot \mathbf{R}') \psi_{rs}(\mathbf{r}') d^3r' d^3R'. \end{aligned} \quad (4.19)$$

Here we have introduced the complete set of two-particle states $|\mathbf{k}\mathbf{K}\rangle = \Omega^{-1} \exp(i\mathbf{K} \cdot \mathbf{R} + i\mathbf{k} \cdot \mathbf{r})$ because Q/e is diagonal in this representation. Expression (4.19) is simplified by integrating over \mathbf{R}' and using the resulting Kronecker delta to perform the summation over \mathbf{K} . Putting the result into the right-hand side of (4.18), and converting the sum over \mathbf{k} to an integral leads to

$$\begin{aligned} \psi_{rs}(\mathbf{r}) &= \exp(i\mathbf{k}_{rs} \cdot \mathbf{r}) - \int K(\mathbf{r}, \mathbf{r}') v(\mathbf{r}') \psi_{rs}(\mathbf{r}') d^3r', \\ &\quad (4.20) \end{aligned}$$

where the kernel $K(\mathbf{r}, \mathbf{r}')$ is given by

$$K(\mathbf{r}, \mathbf{r}') = \int \frac{d^3k}{(2\pi)^3} \frac{Q(\mathbf{k}, \mathbf{K}_{rs})}{e(\mathbf{k}, \mathbf{K}_{rs})} \exp[i\mathbf{k} \cdot (\mathbf{r} - \mathbf{r}')]. \quad (4.21)$$

In these expressions, $K(\mathbf{r}, \mathbf{r}')$ is the kernel of the operator Q/e . To see what is happening, it is helpful to draw a picture in momentum space. Figure 19(a) shows a sphere of radius k_F , and indicates possible values for the relative momentum vector \mathbf{k} and the total momentum vector \mathbf{K}_{rs} . When the two particles interact, the total momentum \mathbf{K}_{rs} remains constant, but the two-body potential can cause a transition from the initial state of relative momentum \mathbf{k}_{rs} to an intermediate state of relative momentum \mathbf{k} , provided the transition is not forbidden by the Pauli operator Q . In the intermediate state, particles 1 and 2 have momenta $\frac{1}{2}\mathbf{K}_{rs} + \mathbf{k}$ and $\frac{1}{2}\mathbf{K}_{rs} - \mathbf{k}$, respectively, and the operator Q requires that both these momenta be above the Fermi sea.

Figure 19(a) is drawn with $k_1 > k_F$ but $k_2 < k_F$. Hence $Q(\mathbf{k}, \mathbf{K}_{rs}) = 0$, and Q annihilates this two-particle intermediate state. Figure 19(b) differs from 19(a) only in the direction of \mathbf{k} , but the resulting intermediate state has both particles above the Fermi sea, and for this state $Q(\mathbf{k}, \mathbf{K}_{rs}) = 1$. We therefore see that

the value of $Q(\mathbf{k}, \mathbf{K}_{rs})$ depends on the magnitude of \mathbf{k} , the magnitude of \mathbf{K}_{rs} , and on the angle between them; and the same is true of $e(\mathbf{k}, \mathbf{K}_{rs})$. Thus Q/e is a rather complicated operator, and this is the main source of difficulty in calculating the reaction matrix.

For a known energy spectrum (that is, for a known dependence of the single-particle energy on momentum), one can in principle evaluate expression (4.21) for $K(\mathbf{r}, \mathbf{r}')$. Then (4.20) becomes a well-defined integral equation for $\psi_{rs}(\mathbf{r})$.

It is now possible to see the connection between our nuclear-matter Schrödinger equation and nucleon–nucleon scattering. The nuclear Schrödinger equation becomes identical with the free-particle scattering equation when it is simplified by replacing the operator Q by unity, and taking the energy $E(k)$ to be pure kinetic energy. Both of these simplifications are appropriate for particles in empty space. Let the relative momentum of the initial two-particle state be \mathbf{k}_0 , and let us calculate $\psi(\mathbf{r})$ on the energy shell so that

$$W = k_0^2 + \frac{1}{4}K_0^2, \quad (4.22)$$

where \mathbf{K}_0 is the total momentum. One then finds that

$$Q(\mathbf{k}, \mathbf{K}_0) = 1, \quad (4.23)$$

$$e(\mathbf{k}, \mathbf{K}_0) = k^2 - k_0^2, \quad (4.24)$$

and it follows that $K(\mathbf{r}, \mathbf{r}')$ is given by

$$\begin{aligned} K(\mathbf{r}, \mathbf{r}') &= \int \frac{d^3k}{(2\pi)^3} \frac{\exp[i\mathbf{k} \cdot (\mathbf{r} - \mathbf{r}')] }{k^2 - k_0^2 - i\epsilon}, \\ &= \frac{\exp(ik_0|\mathbf{r} - \mathbf{r}'|)}{4\pi|\mathbf{r} - \mathbf{r}'|}. \end{aligned} \quad (4.25)$$

The integral equation (4.20) for $\psi(\mathbf{r})$ now becomes

$$\psi(\mathbf{r}) = \exp(i\mathbf{k}_0 \cdot \mathbf{r}) - \frac{1}{4\pi} \int \frac{\exp(ik_0|\mathbf{r} - \mathbf{r}'|)}{|\mathbf{r} - \mathbf{r}'|} v(\mathbf{r}')\psi(\mathbf{r}')d^3r', \quad (4.26)$$

which is the well-known integral equation for two-particle scattering.

In (4.25) we have arbitrarily chosen to add $-i\epsilon$ to the denominator of the integrand in order to obtain an *outgoing* scattered wave. In nuclear matter, however, the singularity at $k=k_0$ would be excluded from the region of integration by the Pauli operator Q . Consequently, for nuclear matter, there is no arbitrariness in the kernel $K(\mathbf{r}, \mathbf{r}')$.

The wave that determines the scattering is the difference between $\psi(\mathbf{r})$ and $\exp(i\mathbf{k}_0 \cdot \mathbf{r})$ and is represented by the integral in Eq. (4.26). At large r this wave behaves like $r^{-1} \exp(ik_0 r)$, a function which contains only momentum components of magnitude k_0 . This is in accord with the requirement of energy conservation in two-particle scattering: outside the range of the potential, the wave function must be

built up from momentum states that have the same energy as the initial state of relative momentum \mathbf{k}_0 . Of course ψ contains components of momentum with magnitude different from k_0 , but these serve only to build up the short-range correlations that are required by the two-body potential; they can never contribute to the scattering.

Momentum components of magnitude k_0 lead to the singularity in the integrand of expression (4.25) for $K(\mathbf{r}, \mathbf{r}')$. This is because the operator e gives zero when applied to such momentum states, and $K(\mathbf{r}, \mathbf{r}')$ represents the operator $1/e$. Thus there is an intimate connection between the asymptotic scattered wave and the singularity in the integrand of formula (4.25). This point has been discussed in detail because one of the most important features of nuclear matter is the *absence* of any singularity in the integrand of (4.21) and the corresponding absence of any scattered wave at large r .

In nuclear matter ψ approaches the unperturbed plane wave so rapidly at large distances that all phase shifts are zero,¹⁵ and there is no scattering at all. This phenomenon is called the “healing” of the two-body wave function.¹⁶ The short-range repulsion forces ψ to go to zero at small r , thus producing a “wound” in the wave function. But the wound heals rapidly at larger r , and the phase shift is zero. This healing comes about because the integrand of formula (4.21) for $K(\mathbf{r}, \mathbf{r}')$ has no singularity. In other words, no energy-conserving momentum components are available for scattering.

Let us look at a specific example in detail. Let two particles in the Fermi sea have equal and opposite momenta of magnitude k_0 , and consider their interaction. For this case the total momentum is zero and the relative momentum of the unperturbed wave function has magnitude $k_{rs} = k_0$. We assume also that G is to be calculated on the energy shell so that $W = 2E(k_0)$. The functions Q and e are clearly given by

$$e(\mathbf{k}, \mathbf{K}_{rs} = 0) = 2E(k) - 2E(k_0), \quad (4.27)$$

$$\begin{aligned} Q(\mathbf{k}, \mathbf{K}_{rs} = 0) &= 1, & k > k_F, \\ &= 0, & k < k_F. \end{aligned} \quad (4.28)$$

Hence $K(\mathbf{r}, \mathbf{r}')$ becomes

$$\begin{aligned} K(\mathbf{r}, \mathbf{r}') &= \int_{k > k_F} \frac{d^3k}{(2\pi)^3} \frac{\exp[i\mathbf{k} \cdot (\mathbf{r} - \mathbf{r}')] }{2E(k) - 2E(k_0)}, \\ &= \frac{4\pi}{(2\pi)^3} \int_{k_F}^{\infty} \frac{k^2 dk}{2E(k) - 2E(k_0)} \frac{\sin k|\mathbf{r} - \mathbf{r}'|}{k|\mathbf{r} - \mathbf{r}'|}. \end{aligned} \quad (4.29)$$

Since $k_0 < k_F < k$, the integrand has no singularity in

¹⁵ H. A. Bethe and J. Goldstone, Proc. Roy. Soc. (London) **A238**, 551 (1957).

¹⁶ L. C. Gomes, J. D. Walecka, and V. F. Weisskopf, Ann. Phys. (N.Y.) **3**, 241 (1958). This paper contains a very helpful discussion of healing, with many interesting figures.

the region of integration. Therefore, there can be no energy-conserving scattering, and the wave function must heal at large r .

To show this mathematically, we integrate by parts to obtain the leading term of $K(\mathbf{r}, \mathbf{r}')$ for large $|\mathbf{r}-\mathbf{r}'|$. The result is

$$K(\mathbf{r}, \mathbf{r}') = \frac{4\pi}{(2\pi)^3} \frac{k_F}{2E(k_F) - 2E(k_0)} \frac{\cos k_F |\mathbf{r}-\mathbf{r}'|}{|\mathbf{r}-\mathbf{r}'|^2} + O(|\mathbf{r}-\mathbf{r}'|^{-3}). \quad (4.30)$$

Putting this result into the integral equation (4.20) for ψ shows that at large r the difference between ψ and the unperturbed plane wave behaves like an oscillating function divided by r^2 . On the other hand, in the L th partial wave, the difference between ψ and the unperturbed wave function falls off only like

$$r^{-1} \{ \sin [k_0 r - \frac{1}{2}(L\pi) + \delta_L] - \sin [k_0 r - \frac{1}{2}(L\pi)] \}, \quad (4.31)$$

where δ_L is the phase shift. Clearly a contradiction can be avoided only if the phase shift vanishes.

Healing occurs in this case because the operator Q excludes the singular point $k=k_0$ from the region of integration. But suppose k_0 had been chosen to be greater than k_F . Then the singularity would not have been excluded, and the result would have been a non-zero phase shift. The flaw in this argument is that when $k_0 > k_F$, we are considering the interaction of two particles *above* the Fermi sea, and such interactions are always computed off the energy shell. The starting energy W is no longer equal to $2E(k_0)$ but takes a value that guarantees that no singularity can occur. In general, then, the healing property results from the fact that there are no vanishing energy denominators in the Brueckner–Goldstone expansion.

V. THE REFERENCE-SPECTRUM METHOD

How does one actually calculate $\psi_{rs}(\mathbf{r})$? Because of the strong short-range repulsion in the nucleon–nucleon potential, it is convenient to work in coordinate space rather than in momentum space. The short-range repulsion is usually approximated by an infinitely repulsive core, and then the single most important property of the correlated wave function is that it vanishes inside the hard core. This condition takes a simple form in coordinate space and a complicated form in momentum space; so coordinate space seems preferable.

The main difficulty in calculating $\psi_{rs}(\mathbf{r})$ comes from the operator Q/e , which is represented in coordinate space by the kernel $K(\mathbf{r}, \mathbf{r}')$. Ordinarily $K(\mathbf{r}, \mathbf{r}')$ can only be evaluated numerically. And even after it has been evaluated, one is still faced with an integral equation for $\psi_{rs}(\mathbf{r})$.

Nevertheless, Brueckner and Gammel¹⁷ successfully attacked the problem in this way in their IBM calculation in 1958. By making two very minor approximations, they decomposed the equation for $\psi_{rs}(\mathbf{r})$ into a set of uncoupled integral equations for the various partial waves of ψ . Each partial-wave component of $K(\mathbf{r}, \mathbf{r}')$ was evaluated numerically, and the integral equation for the corresponding partial wave of ψ was then solved by standard numerical methods.

However, a much better method of calculating the G matrix has recently been developed. This is the reference-spectrum method, which will now be described in some detail. All the material of this section, and much more, can be found in the original paper by Bethe, Brandow, and Petschek.¹⁸

The reference spectrum method has two advantages over the Brueckner–Gammel method. (1) The reference-spectrum method gives a first approximation for G and a systematic way of improving this approximation until any desired accuracy is attained. The approximations of Brueckner and Gammel,¹⁷ although numerically accurate to less than 1 MeV per particle, cannot easily be improved in any systematic way. (2) The reference-spectrum method gives a first approximation which is quite accurate but is still *very easy to compute*, in contrast to the Brueckner–Gammel method which can be carried out only on an electronic computer. The first advantage is not very important, but the second one is crucial because it permits a quantitative study of higher order diagrams.^{2,19–21} Such a study is of course necessary if one is to investigate the convergence of the Brueckner–Goldstone expansion.

In order to understand the reference-spectrum method, it is helpful to return to our original equation for the correlated wave function:

$$\Psi_{rs}(\mathbf{r}_1, \mathbf{r}_2) = \Phi_{rs}(\mathbf{r}_1, \mathbf{r}_2) - (Q/e)v\Psi_{rs}(\mathbf{r}_1, \mathbf{r}_2). \quad (5.1)$$

The basic idea is to approximate the operator Q/e by a simpler one. First, consider the operator e , which is defined by

$$e |pq\rangle = [E(k_p) + E(k_q) - W] |pq\rangle, \quad (5.2)$$

where $|pq\rangle$ is a product of two plane waves. Suppose the energy spectrum $E(k)$ for which the G matrix is to be calculated were approximated by a “reference” spectrum $E^R(k)$ defined by

$$E^R(k) = k^2/2m^* + A_2, \quad (5.3)$$

where A_2 and the dimensionless effective mass m^*

¹⁷ K. A. Brueckner and J. L. Gammel, Phys. Rev. **109**, 1023 (1958).

¹⁸ H. A. Bethe, B. H. Brandow, and A. G. Petschek, Phys. Rev. **129**, 225 (1963). This paper, and its authors, will be referred to as BBP.

¹⁹ R. Rajaraman, Phys. Rev. **129**, 265 (1963).

²⁰ R. Rajaraman, Phys. Rev. **131**, 1244 (1963).

²¹ H. A. Bethe, Phys. Rev. **138**, B804 (1965).

are constants. The corresponding reference approximation for e could then be written

$$e^R = -(2m^*)^{-1}(\nabla_1^2 + \nabla_2^2) + 2A_2 - W \quad (5.4)$$

because, when applied to $|pq\rangle$, this operator gives

$$[(2m^*)^{-1}(k_p^2 + k_q^2) + 2A_2 - W] |pq\rangle = [E^R(k_p) + E^R(k_q) - W] |pq\rangle. \quad (5.5)$$

This approximate form for e is very convenient because it will allow us to write a differential equation for Ψ_{rs} instead of an integral equation.

However, a previous question is whether or not $E(k)$ can be well approximated by a quadratic function of k . The answer to this question depends on the choice of the potential energy $U(k)$. The function $U(k)$ is at our disposal and is to be chosen in such a way that the Brueckner–Goldstone expansion converges well. The currently accepted choice of $U(k)$, which will be discussed in Sec. VI, leads to an energy spectrum $E(k)$ similar to that given by the solid curve in Fig. 20. The discontinuity at $k = k_F$ is in no way related to the energy gap of superconductivity.

The energy spectrum $E(k)$ cannot be well represented by a quadratic over the entire range of k , but a good fit with a quadratic may be obtained in restricted regions of momentum space. For two interesting regions, the parameters m^* and A_2 that give a good fit to $E(k)$ are

$$\begin{aligned} 0 < k < k_F: & \quad m^* \sim 0.6, \quad A_2 \sim -100 \text{ MeV}, \\ 3F^{-1} < k < 5F^{-1}: & \quad m^* \sim 1.0, \quad A_2 \sim 0. \end{aligned} \quad (5.6)$$

These are just rough values, but it is clear that the two sets of parameters are completely different. Thus it is important to select the particular region of k space in which $E(k)$ is to be fitted.

One important fact is clear: Once the starting energy W has been chosen, the energy spectrum of states in the Fermi sea is completely irrelevant for the purpose of computing the G matrix. The reason is that in Eq. (5.1) for the correlated wave function, the presence of

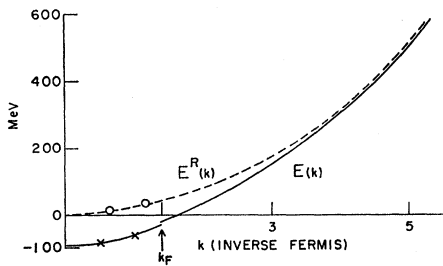


FIG. 20. Typical plot of the energy spectrum $E(k)$ used in nuclear matter (solid curve). The dashed curve represents the reference spectrum $E^R(k)$, which is chosen to approximate the actual spectrum in the range $3F^{-1} < k < 5F^{-1}$.

the operator Q allows $1/e$ to operate only on two-particle states in which both particles are *outside* the Fermi sea. For a given value of W , therefore, the operator Q/e depends only on the behavior of the function $E(k)$ in the region $k > k_F$.

As will be seen later, in calculating the G matrix the region in which it is most important to have a good representation for $E(k)$ is from $k = 3F^{-1}$ to $k = 5F^{-1}$. Hence the reference spectrum $E^R(k)$ is chosen to fit the true spectrum as well as possible in this important region.¹⁸ The result is the dashed curve shown in Fig. 20.

The first step, then, in the reference-spectrum method is to replace e by the operator e^R given by formula (5.4). In this expression the value of the starting energy W is to be calculated from the actual energy spectrum, not from the reference spectrum. For a given pair of interacting particles, W is just a single number and there is no need to approximate it in any way.

The reference spectrum $E^R(k)$ is clearly a very bad approximation to the actual spectrum for states in the Fermi sea. As was pointed out before, this fact is not disturbing. On the contrary, it allows us to make the tremendous simplification of replacing the operator Q by unity without introducing much additional error into the G matrix. Replacing Q by unity, which is the second step in the derivation of the reference-spectrum method, leads to the equation

$$\Psi_{rs}^R = \Phi_{rs} - (e^R)^{-1} v \Psi_{rs}^R \quad (5.7)$$

for the reference wave function Ψ_{rs}^R . The first approximation of the reference-spectrum method amounts to replacing Ψ_{rs} by Ψ_{rs}^R in Eq. (4.15) for the G matrix.

There are two reasons why replacing Q by unity does not cause serious error. First of all, applying $1/e^R$ to any of the states forbidden by Q gives a rather small result. For the on-energy-shell interaction of two particles in the Fermi sea, this can be seen by studying Fig. 20. Suppose the two interacting particles are initially in the states represented by the crosses shown in Fig. 20. Then a typical two-particle state into which the initial state is forbidden to scatter is represented by the two circles. The operator e^R gives the difference between the *reference* energy of the forbidden state and the correct energy of the initial state. As can be seen from Fig. 20, this energy difference is likely to be fairly large, say 100 MeV. The worst possible case is when the two crosses are both at $k = k_F$ and both circles are at $k = 0$, and even then the value of e^R is as large as $-2E(k_F) \approx +50$ MeV.

Thus $1/e^R$ is always reasonably small. In particular, it has no singularity and therefore the reference wave function heals at large distances. If $1/e^R$ had a singularity, then the reference wave function would have a nonzero phase shift and would be qualitatively different from the correct wave function. It is very fortunate that fitting $E^R(k)$ to $E(k)$ for k between $3F^{-1}$ and

5 F^{-1} leads to an operator e^R that preserves the healing property.

The second reason why putting $Q=1$ allows a good approximation to the G matrix is that the number of states forbidden by Q is only a small fraction of the total number of states of importance in the calculation of Ψ_{rs} . That is, Q affects only momenta less than $k_F=1.36 F^{-1}$, while momenta all the way up to $5 F^{-1}$ play a role in the determination of the correlated wave function.¹⁸ So the important region in phase space is a sphere of radius $5 F^{-1}$, and the volume of this region is 40 times the volume of the Fermi sphere, which is the region of phase space affected by Q .

The reference-spectrum method can be briefly summarized as follows. The reference G matrix G^R is obtained from the correct G matrix by replacing Q/e by $1/e^R$. Hence G^R satisfies

$$G^R = v - v(e^R)^{-1}G^R. \tag{5.8}$$

To evaluate G^R , the equation

$$\Psi_{rs}^R = \Phi_{rs} - (e^R)^{-1}v\Psi_{rs}^R \tag{5.9}$$

is solved for the correlated reference wave function Ψ_{rs}^R , which then is substituted in

$$\langle pq | G^R | rs \rangle = \langle \Phi_{pq} | v | \Psi_{rs}^R \rangle. \tag{5.10}$$

After G^R has been calculated, a better approximation for G may be obtained by iterating the *exact* equation

$$G = G^R + G^R[(e^R)^{-1} - (Q/e)]G, \tag{5.11}$$

which is derived in Appendix A of the BBP paper. Thus G^R is the first approximation in a systematic expansion of G . This expansion is extremely useful because the leading term G^R is both simple and accurate. For a central two-body potential, the diagonal matrix element of G that describes the interaction of two particles in the Fermi sea is given correctly by G^R to within about 5%,¹⁸ corresponding to an error of 2–3 MeV per particle. The situation is not so favorable for a tensor force,^{18,22,23} for which the error is roughly 15%.

We now turn to the details of calculating G^R . Equation (5.9) for Ψ_{rs}^R can be written in the form

$$e^R Z_{rs}^R = v\Psi_{rs}^R, \tag{5.12}$$

where

$$Z_{rs}^R = \Phi_{rs} - \Psi_{rs}^R. \tag{5.13}$$

The volume and center-of-mass dependences of the two-body wave functions are separated out in the usual

²² D. W. L. Sprung, P. C. Bhargava, and T. K. Dahlblom, *Phys. Letters* **21**, 538 (1966).

²³ D. W. L. Sprung and P. C. Bhargava, *Ann. Phys. (N.Y.)* **42**, 222 (1967).

way. We write

$$\left. \begin{matrix} \Phi_{rs} \\ \Psi_{rs}^R \\ Z_{rs}^R \end{matrix} \right\} = \Omega^{-1} \exp(i\mathbf{K}_{rs} \cdot \mathbf{R}) \left\{ \begin{matrix} \phi_{rs}(\mathbf{r}) \\ \psi_{rs}^R(\mathbf{r}) \\ \zeta_{rs}^R(\mathbf{r}) \end{matrix} \right\}, \tag{5.14}$$

where $\zeta_{rs}^R = \phi_{rs} - \psi_{rs}^R$, and $\phi_{rs}(\mathbf{r}) = \exp(i\mathbf{k}_{rs} \cdot \mathbf{r})$. Since e^R can be written

$$e^R = -(m^*)^{-1}(\nabla_r^2 + \frac{1}{4}\nabla_R^2) + 2A_2 - W, \tag{5.15}$$

it follows that

$$\begin{aligned} &[-(m^*)^{-1}(\nabla_r^2 + \frac{1}{4}\nabla_R^2) + 2A_2 - W]\Omega^{-1} \\ &\quad \times \exp(i\mathbf{K}_{rs} \cdot \mathbf{R})\zeta_{rs}^R(\mathbf{r}) \\ &= v\Omega^{-1} \exp(i\mathbf{K}_{rs} \cdot \mathbf{R})\psi_{rs}^R(\mathbf{r}). \end{aligned} \tag{5.16}$$

This leads to

$$(\nabla_r^2 - \gamma^2)\zeta_{rs}^R(\mathbf{r}) = -m^*v\psi_{rs}^R(\mathbf{r}), \tag{5.17}$$

where

$$\gamma^2 = \frac{1}{4}K_{rs}^2 + m^*(2A_2 - W). \tag{5.18}$$

Equation (5.17) is called the reference wave equation, and solving it is no more difficult than solving the equation for free-particle scattering. Since $\psi_{rs}^R(\mathbf{r})$ must vanish inside the hard core and must approach ϕ_{rs} for large r , the boundary conditions for the difference function ζ_{rs}^R are

$$\begin{aligned} \zeta_{rs}^R &= \phi_{rs} && \text{for } r \leq c, \\ &= 0 && \text{as } r \rightarrow \infty. \end{aligned} \tag{5.19}$$

The constant γ^2 is seen to be positive, and this fact ensures healing. As $r \rightarrow \infty$, ζ^R falls off like $\exp(-\gamma r)$ or $v(r)$, whichever decreases more slowly.

The above derivation of the reference wave equation is the usual one, but we could just as well start from the integral equation (4.20) for $\psi_{rs}(\mathbf{r})$. When Q/e is replaced by $1/e^R$, the functions $Q(\mathbf{k}, \mathbf{K})$ and $e(\mathbf{k}, \mathbf{K})$ become

$$Q(\mathbf{k}, \mathbf{K}) = 1, \tag{5.20}$$

$$e(\mathbf{k}, \mathbf{K}) = (m^*)^{-1}(k^2 + \gamma^2), \tag{5.21}$$

and the kernel $K(\mathbf{r}, \mathbf{r}')$ is given by

$$\begin{aligned} K(\mathbf{r}, \mathbf{r}') &= m^* \int \frac{d^3k}{(2\pi)^3} \frac{\exp[i\mathbf{k} \cdot (\mathbf{r} - \mathbf{r}')] }{k^2 + \gamma^2}, \\ &= m^* \frac{\exp(-\gamma |\mathbf{r} - \mathbf{r}'|)}{4\pi |\mathbf{r} - \mathbf{r}'|}. \end{aligned} \tag{5.22}$$

Putting this value of $K(\mathbf{r}, \mathbf{r}')$ into the integral equation (4.20) for $\psi_{rs}(\mathbf{r})$, and using

$$(\nabla^2 - \gamma^2)K(\mathbf{r}, \mathbf{r}') = -m^*\delta(\mathbf{r} - \mathbf{r}'), \tag{5.23}$$

leads immediately to the reference wave equation.

To solve the reference wave equation, we introduce partial waves by means of

$$\left. \begin{matrix} \phi_{rs}(\mathbf{r}) \\ \psi_{rs}^R(\mathbf{r}) \\ \zeta_{rs}^R(\mathbf{r}) \end{matrix} \right\} = \sum_L i^L [4\pi(2L+1)]^{1/2} (k_0 r)^{-1} \left\{ \begin{matrix} \mathcal{G}_L(r) \\ u_L(r) \\ \chi_L(r) \end{matrix} \right\} \times Y_{L0}(\hat{k}_0, \hat{r}). \quad (5.24)$$

On the right-hand side, the initial relative momentum k_{rs} has been denoted by k_0 . Although it is not explicitly indicated, the partial-wave amplitudes $u_L(r)$ and $\chi_L(r)$ depend on k_0 , K_{rs} , and W . The function $\mathcal{G}_L(r)$ is defined by

$$\mathcal{G}_L(r) = k_0 r j_L(k_0 r), \quad (5.25)$$

where j_L is a spherical Bessel function. Putting the partial-wave expansions into the reference wave equation gives

$$\left[\frac{d^2}{dr^2} - \frac{L(L+1)}{r^2} - \gamma^2 \right] \chi_L(r) = -m^* v(r) u_L(r), \quad (5.26)$$

with the boundary conditions

$$\begin{aligned} \chi_L(r) &= \mathcal{G}_L(r) & \text{for } r \leq c, \\ &= 0 & \text{as } r \rightarrow \infty. \end{aligned} \quad (5.27)$$

Although we have here assumed a spherically symmetric potential, all the formulas can easily be modified to include the effects of the tensor force.^{17,18}

Let us now examine the behavior of the S -wave solutions of Eq. (5.26). Suppose first that the potential consists only of a hard core, with no attractive part whatever, i.e.,

$$\begin{aligned} v(r) &= +\infty & \text{for } r \leq c, \\ &= 0 & \text{for } r > c. \end{aligned} \quad (5.28)$$

Then the solution for χ_0 that satisfies all boundary conditions is

$$\begin{aligned} \chi_0(r) &= \mathcal{G}_0(r) = \sin k_0 r & \text{for } r \leq c, \\ &= \mathcal{G}_0(c) \exp[-\gamma(r-c)] & \text{for } r > c. \end{aligned} \quad (5.29)$$

A plot of \mathcal{G}_0 , u_0 , and χ_0 is shown in Fig. 21; the initial relative momentum k_0 has been assumed to be 1.0 F^{-1} , which is a typical value for two particles in the Fermi sea.

A measure of the healing distance is $1/\gamma$, which is typically about 0.7 F for the interaction of two particles in the Fermi sea. The larger the value of γ , the more rapid is the healing. The physical reason for this is that $\phi - \psi^R = (1/e^R)v\psi^R$, and increasing γ makes e^R larger; hence each virtual transition produced by v involves a larger jump in energy. Thus γ is a measure of the "stiffness" of the wave function against deviating from ϕ in response to the two-body potential. Of course, γ

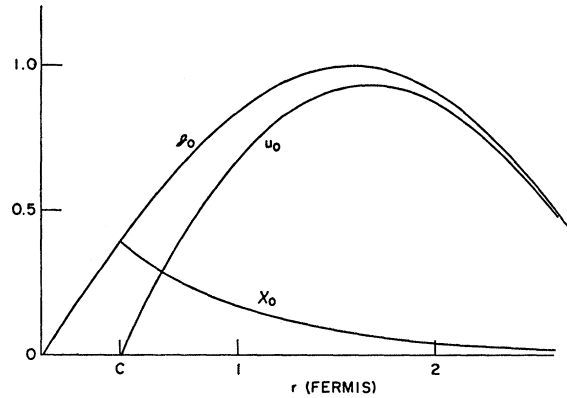


FIG. 21. Relative S -wave functions for a pure hard-core potential. Inside the core, $\chi_0 = \mathcal{G}_0$ and $u_0 = 0$. The parameters used are $c = 0.4 \text{ F}$, $k_0 = 1.0 \text{ F}^{-1}$, $\gamma = 1.4 \text{ F}^{-1}$.

cannot compete against the infinitely strong hard core, and u_0 therefore vanishes for $r \leq c$. But outside the core, where v is weaker (in fact $v = 0$ for $r > c$ in the present case), γ produces rapid healing.

To illustrate the effect of putting in an attractive force outside the hard core, the reference wave equation has been solved for the case of the standard hard-core potential (SHCP) of Moszkowski and Scott.²⁴ This potential, which has a single bound state at zero energy and an effective range of 2.5 F , is defined by

$$\begin{aligned} v(r) &= +\infty & \text{for } r < c, \\ &= -v_0 \exp[-\mu(r-c)] & \text{for } r > c, \end{aligned} \quad (5.30)$$

$$v_0 = 260 \text{ MeV}, \quad c = 0.4 \text{ F}, \quad \mu = 2.083 \text{ F}^{-1}. \quad (5.31)$$

The SHCP has a hard core of about the right size, and the attractive force in the outer region is of reasonable strength and range. Moreover, it leads to wave functions and matrix elements that are similar to those obtained from more realistic, and therefore more complicated, potentials.

When v contains an attraction outside the hard core, Eq. (5.26) shows that $d^2\chi_0/dr^2$ will be increased in the region $r > c$. This causes χ_0 to decrease more rapidly just outside the core, and in fact χ_0 soon becomes negative and approaches zero through negative values when r goes to infinity, as shown in Fig. 22. Putting in the attractive part of v causes u_0 to "overshoot" \mathcal{G}_0 , but the resulting u_0 is not much different from that obtained with the hard core alone. In this sense the attractive part of the nuclear two-body force is rather weak. We will see later that the weakness of the attractive force is essential for the convergence of the energy expansion.

The assertion that $E^R(k)$ should be fitted to $E(k)$ in the region $3 \text{ F}^{-1} < k < 5 \text{ F}^{-1}$ can now be made plausi-

²⁴ S. A. Moszkowski and B. L. Scott, *Ann. Phys. (N.Y.)* **11**, 65 (1960).

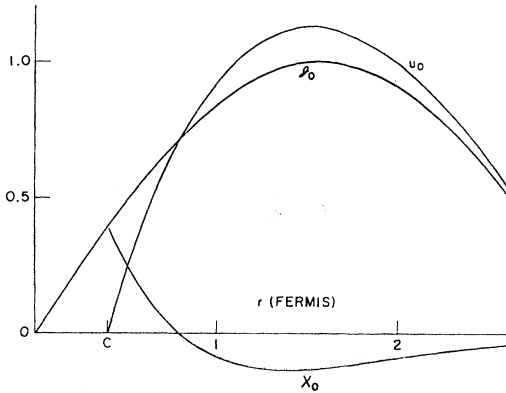


FIG. 22. Relative *S*-wave functions for the standard hard-core potential, with $k_0=1.0 \text{ F}^{-1}$ and $\gamma=1.68 \text{ F}^{-1}$. Inside the hard core, $\chi_0=g_0$ and $u_0=0$.

ble.¹⁸ The point is that $e(\mathbf{k}, \mathbf{K})$ should be accurately approximated in the region of relative momentum space where the Fourier components of $(Q/e)v\psi(\mathbf{r})$ are large. However, $(Q/e)v\psi(\mathbf{r})$ is approximately equal to $\zeta^R(\mathbf{r})$, and the Fourier transform of the *S*-wave part of $\zeta^R(\mathbf{r})$ is proportional to

$$F_0(k) = k_0^{-1} \int_0^\infty \sin kr \chi_0(r) dr. \quad (5.32)$$

From the plot of $\chi_0(r)$ in Fig. 22, it is clear that this integral will be near its maximum value when $\sin kr$ has its first maximum at the core edge, i.e., when

$$k = \pi/2c \approx 4 \text{ F}^{-1}. \quad (5.33)$$

If the total momentum is zero, a relative momentum of 4 F^{-1} corresponds to the virtual excitation of two particles with equal and opposite momenta of magnitude 4 F^{-1} . Thus 4 F^{-1} is a typical single-particle momentum for which $E^R(k)$ should accurately approximate $E(k)$. The repulsive core is, of course, the feature that is responsible for exciting Fourier components of such high energy (a nucleon of momentum 4 F^{-1} has a kinetic energy of 330 MeV). We have considered only *S* waves with total momentum zero, but for the interaction of two particles in the Fermi sea this is sensible for the following reasons. First, the total momentum is usually much less than 4 F^{-1} . Second, higher partial waves have very small difference functions χ_L because the initial relative momentum is so low that the centrifugal barrier prevents the unperturbed wave function $g_L(r)$ from “seeing” the hard core.

After the reference wave function has been found, G^R is calculated from Eq. (4.17), which can be written in terms of partial waves as

$$\langle \mathbf{k}_0 | G | \mathbf{k}_0 \rangle = 4\pi \sum_L (2L+1) \frac{1}{k_0^2} \int_0^\infty g_L v u_L dr. \quad (5.34)$$

For simplicity we consider only the diagonal matrix

element. This formula cannot be used in its present form because $v = \infty$, $u_L = 0$ inside the hard core, and it is not clear what value should be assigned to the product of these two quantities. BBP overcome this difficulty by manipulating the differential equations

$$\{ (d^2/dr^2) - [L(L+1)/r^2] + k_0^2 \} g_L = 0, \quad (5.35)$$

$$\{ (d^2/dr^2) - [L(L+1)/r^2] - \gamma^2 \} \chi_L = -m^* v u_L, \quad (5.36)$$

$$\{ (d^2/dr^2) - [L(L+1)/r^2] - \gamma^2 \} \mathcal{C}_L = 0. \quad (5.37)$$

The function $\mathcal{C}_L(r)$ is the solution for χ_L for the case of a pure-hard-core potential and can be calculated analytically. Equations (5.35) and (5.36) are valid for all r , but Eq. (5.37) is used only in the region $r > c$.

Multiplying (5.35) by χ_L , (5.36) by g_L and subtracting gives

$$\frac{d}{dr} \left(\chi_L \frac{dg_L}{dr} - g_L \frac{d\chi_L}{dr} \right) + (\gamma^2 + k_0^2) g_L \chi_L = m^* g_L v u_L. \quad (5.38)$$

We integrate this from 0 to $c+$, using the fact that $\chi_L = g_L$ inside the hard core, and obtain

$$\int_0^{c+} g_L v u_L dr = \frac{\gamma^2 + k_0^2}{m^*} \int_0^c g_L^2 dr + \frac{g_L(c)}{m^*} \left(\frac{dg_L}{dr} - \frac{d\chi_L}{dr} \right)_{r=c+}. \quad (5.39)$$

Since $u_L = g_L - \chi_L$, the last term on the right-hand side is proportional to the slope of u_L at the core edge. It is convenient to write $(d\chi_L/dr)_{r=c+}$ in the form

$$\frac{g_L(c)}{m^*} \frac{d\chi_L}{dr} \Big|_{c+} = \frac{g_L(c)}{m^*} \frac{d\mathcal{C}_L}{dr} \Big|_{c+} + \int_{c+}^\infty \mathcal{C}_L v u_L dr, \quad (5.40)$$

which is obtained by combining Eqs. (5.36) and (5.37) and integrating from $c+$ to ∞ . When this replacement is made in (5.39), the reference *G* matrix takes the form

$$\langle \mathbf{k}_0 | G^R | \mathbf{k}_0 \rangle = \frac{4\pi}{k_0^2} \sum_L (2L+1) \left\{ \frac{\gamma^2 + k_0^2}{m^*} \int_0^c g_L^2 dr + \frac{g_L(c)}{m^*} \left(\frac{dg_L}{dr} - \frac{d\mathcal{C}_L}{dr} \right)_{r=c} + \int_c^\infty (g_L - \mathcal{C}_L) v u_L dr \right\}. \quad (5.41)$$

The first term is called the core volume term, the second is the core boundary term, and the third is called the outer term. For a pure hard core, only the first two terms contribute, and they can be calculated analytically. For the interaction of an average pair in the Fermi sea, the core volume term is usually less than 1 F , the core boundary term is typically $+10 \text{ F}$, and the outer term might be -20 F . For the on-energy-shell interaction of two particles in the Fermi sea, the repulsive terms are nearly independent of the relative momentum k_0 , but the magnitude of the outer term decreases with k_0 . A plot of $\langle \mathbf{k}_0 | G^R | \mathbf{k}_0 \rangle$ vs k_0 , calculated

for the SHCP, is shown in Fig. 23. (The value of $\langle \mathbf{k}_0 | G^R | \mathbf{k}_0 \rangle$ also depends on the *total* momentum, but this dependence is weak.)

An interesting idea due to Brandow²⁵ is to use formula (5.41) to obtain an effective interaction between the pair of interacting particles. The effective interaction $g_L(r)$ in the L th partial wave is defined by requiring that

$$\langle \mathbf{k}_0 | G | \mathbf{k}_0 \rangle = \frac{4\pi}{k_0^2} \sum_L (2L+1) \int_0^\infty g_L^2 g_L(r) dr. \quad (5.42)$$

In the reference spectrum approximation, a function $g_L(r)$ which satisfies this equation is

$$\begin{aligned} g_L(r) &= \frac{\gamma^2 + k_0^2}{m^*} && \text{for } r < c, \\ &= \frac{1}{m^* g_L(c)} \left(\frac{d g_L}{dr} - \frac{d^2 \mathcal{C}_L}{dr^2} \right)_{r=c} \delta(r-c) && \text{for } r = c, \\ &= v(r) \left(1 - \frac{\mathcal{C}_L}{g_L} \right) \frac{u_L}{g_L} && \text{for } r > c. \end{aligned} \quad (5.43)$$

This function is plotted in Fig. 24 for the S state, with the two-body potential taken to be the SHCP. Clearly $g_0(r)$ is completely different from $v(r)$ at small distances. However, because of the healing property, $g_0(r)$ agrees very well with $v(r)$ beyond $r=1$ F.

The separation method for calculating G , invented by Moszkowski and Scott,²⁴ leads to a different effective interaction. For the S state, it is given by

$$\begin{aligned} g_0(r) &= 0 && \text{for } r < d, \\ &= v(r) && \text{for } r > d, \end{aligned} \quad (5.44)$$

where the separation distance d is about 1 F. This interaction is different from formula (5.43); but this does not mean that one of the two is wrong, because our

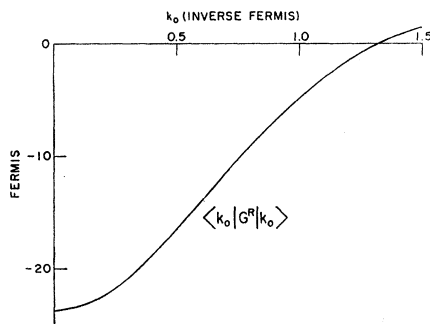


FIG. 23. The diagonal matrix element of G^R as a function of the relative momentum k_0 . The two-body interaction was taken to be the standard hard-core potential, acting only in relative S states. More realistic potentials give very similar results.

²⁵ B. H. Brandow, *Proceedings of the International School of Physics "Enrico Fermi,"* Course 36, Varenna, 1965 (to be published).

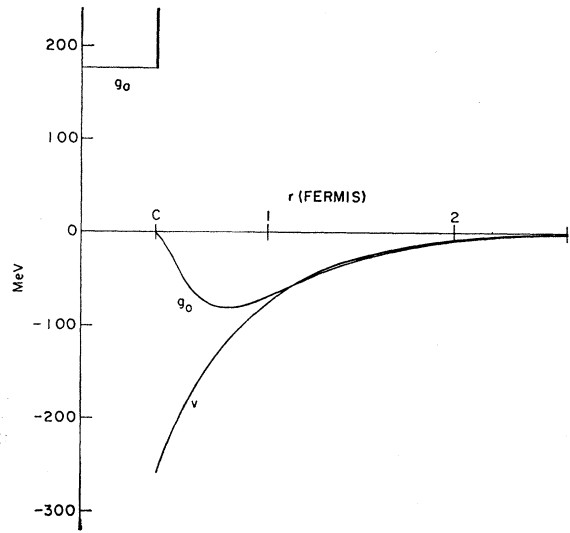


FIG. 24. Brandow's effective interaction in the relative S state, calculated for the standard hard-core potential with $k_0 = 1.0$ F⁻¹, $\gamma = 1.68$ F⁻¹. The heavy vertical line at $r = c$ represents the repulsive delta function at the core edge. The two-body potential is also shown for $r > c$. The behavior of $g_0(r)$ is very similar for all reasonably small values of k_0 .

definition of $g_L(r)$ is not unique. We have only required that $g_L(r)$ lead to the correct value for the integral in Eq. (5.42), and there are obviously many functions $g_L(r)$ that will do this.

The separation method is especially useful for problems involving diagonal matrix elements of G for particles in the Fermi sea, e.g., the calculation of matrix elements to be used in a shell-model calculation. But in the higher order diagrams of the Brueckner-Goldstone expansion, there appear off-diagonal and off-energy-shell matrix elements, and for these the reference-spectrum method is indispensable. (It is also possible and useful to combine the reference-spectrum method with the separation method. See Refs. 2 and 18.)

One can go quite far analytically with the reference-spectrum method. Of course, for exact numerical results a computer is still necessary. But one can make estimates and get a feeling for orders of magnitude by purely analytical methods. Many examples are given in the BBP paper, which presents a wealth of interesting and important material.²

VI. SINGLE-PARTICLE ENERGIES AND CONVERGENCE

It has already been pointed out that the single-particle potential energy $U(k)$ is at our disposal; it is to be chosen with a view towards making the summation of the Brueckner-Goldstone series as easy as possible.

Certain diagrams contain U interactions, and if $U(k)$ is appropriately defined, these diagrams may cancel other diagrams. This cancellation reduces the number of diagrams that must be explicitly evaluated.

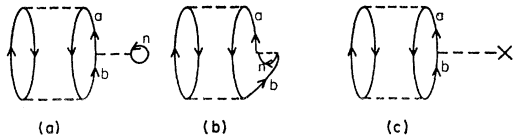


FIG. 25. Three Goldstone diagrams whose sum is zero when the Hartree-Fock definition of the single-particle potential energy is used.

This is the basic idea underlying any definition of $U(k)$. How one chooses $U(k)$ therefore depends on which diagrams one decides to cancel by this choice.

In making this decision, one should keep two points in mind. First, only certain types of diagrams are conveniently canceled by diagrams involving $U(k)$. Second, choosing U to cancel the maximum number of diagrams is not necessarily the best procedure. One should have an idea of which diagrams are appreciable and which are negligible. Then U should be defined so as to cancel as many of the *important* diagrams as possible. We therefore see that the choice of U is closely related to the question of the convergence of the Brueckner-Goldstone expansion.

The most familiar example of a single-particle potential is the Hartree-Fock potential U_{HF} . For a (not necessarily infinite) many-body system with a non-singular two-particle potential v , the Hartree-Fock potential is defined by

$$\langle p | U_{\text{HF}} | q \rangle = \sum_{n \leq A} (\langle pn | v | qn \rangle - \langle pn | v | nq \rangle). \quad (6.1)$$

This definition arises from the requirement that the expectation value of H in the unperturbed ground state be stationary with respect to variation of the single-particle wave functions.

However, this choice of U also has a simple interpretation in terms of Goldstone diagrams. Consider, for example, the three diagrams of Fig. 25. Each of these gives exactly the same contribution except for the matrix element of the middle interaction which is

$$\sum_{n \leq A} \langle an | v | bn \rangle, \quad (6.2)$$

$$- \sum_{n \leq A} \langle an | v | nb \rangle, \quad (6.3)$$

$$- \langle a | U | b \rangle \quad (6.4)$$

for diagrams (a), (b), and (c), respectively. [The last two matrix elements have negative signs because, according to the sign rule $(-1)^{l+l'+e+u}$, diagrams (b) and (c) have the sign opposite to that of diagram (a).] With the Hartree-Fock choice for U , the sum of the three matrix elements is zero, and therefore none of these diagrams need to be considered in summing the Goldstone expansion.

Similarly, one sees that any diagram in which a bubble is attached to a hole line, rather than to a particle line, is canceled by a corresponding diagram involving U . In fact, the Hartree-Fock choice of U en-

sures the exact cancellation of all diagrams containing one or more bubble interactions, exchange bubbles, or U interactions.

Thus the Hartree-Fock definition of U causes the cancellation of a special class of "self-energy" diagrams. For a finite system, this choice of U leads to the familiar Hartree-Fock self-consistency condition. The single-particle wave functions $\phi_p(\mathbf{r})$ which are obtained as solutions of the equation $(T + U_{\text{HF}})\phi_p(\mathbf{r}) = E_p\phi_p(\mathbf{r})$ must agree with the single-particle wave functions used in the calculation of U_{HF} from formula (6.1). For an infinite system, on the other hand, the one-particle wave functions are known from the beginning to be plane waves. The self-consistency condition then becomes trivial, and formula (6.1) merely provides an expression for $\langle q | U_{\text{HF}} | q \rangle = U(k_q)$. (Note that $\langle p | U_{\text{HF}} | q \rangle$ vanishes because of momentum conservation, if \mathbf{k}_p is different from \mathbf{k}_q .)

We now turn to nuclear matter and consider first the definition of $U(k)$ for momenta k_m in the Fermi sea. Suppose that $U(k_m)$ is chosen by analogy with Hartree-Fock theory, i.e., require the cancellation of the three diagrams of Fig. 26. Then we get

$$U(k_m) = \sum_{n \leq A} \langle mn | G(W) | mn \rangle, \quad (6.5)$$

where the exchange term has been omitted because all the important ideas can be illustrated by means of the direct term alone.

Using G matrices instead of v matrices raises the question of what value should be used for the starting energy W . To calculate W , we draw the second-order ladder diagram corresponding to the G matrix of interest, as shown in Fig. 27(a). The energy denominator at the level indicated by the arrow is obtained by applying the operator e to $|cd\rangle$ and is therefore equal to $(E_c + E_d - W)$. But since this energy denominator must also be equal to the sum of the particle energies minus the sum of the hole energies, we find that

$$E_c + E_d - W = E_a + E_b + E_c + E_d - E_i - 2E_m - E_n,$$

$$W = E_m + E_n - (E_a + E_b - E_i - E_m). \quad (6.6)$$

Thus $\langle mn | G | mn \rangle$ is off the energy shell by an amount $(E_a + E_b - E_i - E_m)$. This is undesirable because, if $U(k_m)$ is to be a well-defined function of k_m , then the starting energy W used in Eq. (6.5) can at most depend on m and n .

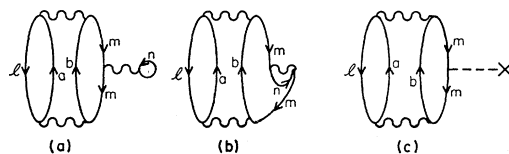


FIG. 26. G -matrix diagrams that occur in the Hartree-Fock definition of $U(k_m)$ for nuclear matter. They are analogous to the v -matrix diagrams of Fig. 25.

The situation is saved, however, by including diagram 27(b) along with 27(a). The matrix elements and the top two energy denominators in these diagrams are identical. Their contributions differ only in the value of the lowest energy denominator. The contribution of the *sum* of both diagrams, apart from the product of four matrix elements of v which is common to the diagrams, is

$$\begin{aligned} & (E_a + E_b - E_l - E_m)^{-1} \\ & \times (E_a + E_b + E_c + E_d - E_l - 2E_m - E_n)^{-1} \\ & \times [(E_a + E_b - E_l - E_m)^{-1} + (E_c + E_d - E_m - E_n)^{-1}] \\ & = (E_a + E_b - E_l - E_m)^{-1} \times (E_c + E_d - E_m - E_n)^{-1} \\ & \times (E_a + E_b - E_l - E_m)^{-1}. \quad (6.7) \end{aligned}$$

Hence the total contribution of both diagrams is equal to the contribution of Fig. 27(a) alone, with the proviso that W should have its on-energy-shell value ($E_m + E_n$) for the purpose of calculating the middle energy denominator.

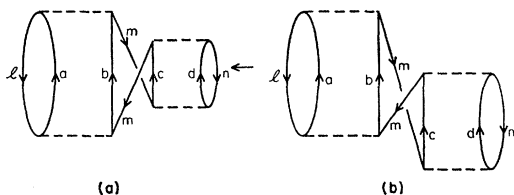


FIG. 27. Diagrams that arise in the definition of $U(k_m)$. (a) The v -matrix ladder diagram that is used to determine the starting energy for the middle G matrix of Fig. 26(a). (b) The diagram which, when combined with diagram 27(a), puts the middle energy denominator on the energy shell.

This remarkable property of v -matrix diagrams was first pointed out by Brueckner and Goldman.²⁶ Before this result can be applied to G -matrix diagrams, it must be generalized—as was done in a simple way by BBP, who prove the result illustrated in Fig. 28. Diagrams 28(a) and 28(b) stand for all possible v -matrix diagrams of the type shown, the only restrictions being that interaction A must be below interaction B, and interaction B must be below interaction C. This vast collection of diagrams is exactly summed by evaluating the single G -matrix diagram 28(c), with the proviso that the middle G matrix be calculated *on the energy shell*. In terms of G matrices with conventional Brueckner-Goldstone energy denominators, the diagrams that are summed in this way form a sequence whose first few members are shown in Fig. 29. Note that two successive G matrices never appear between the same pair of particle lines; this would lead to a redundant ladder diagram.

²⁶ K. A. Brueckner and D. T. Goldman, Phys. Rev. **117**, 207 (1960).

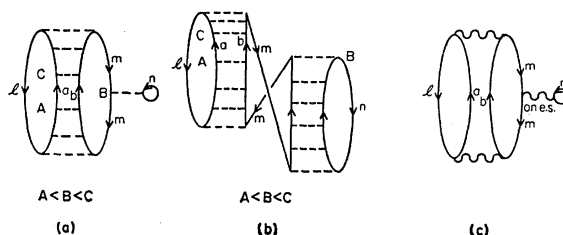


FIG. 28. Diagrams illustrating the generalization of the Brueckner-Goldman result to G -matrix diagrams. All diagrams that can be drawn in the form of 28(a) or 28(b) are exactly summed by the diagram of 28(c), with the middle G matrix calculated on the energy shell.

The single-particle potential for states in the Fermi sea is now defined by means of the *on-energy-shell* G matrix that appears in the diagram of Fig. 28(c), i.e.,

$$U(k_m) = \sum_{n \leq A} \langle mn | G(W = E_m + E_n) | mn \rangle. \quad (6.8)$$

This offers the convenience of working with an on-energy-shell G matrix, and the resulting $U(k_m)$ cancels not just the original diagram of Fig. 26(a) but rather an entire class of diagrams, the first few of which are shown in Fig. 29.

Even though the single-particle wave functions in nuclear matter are known to be plane waves, a non-trivial self-consistency problem arises from the definition of $U(k_m)$ because the G matrix depends on $U(k_m)$ through the starting energy. Starting with any function $U(k_m)$, one can evaluate the matrix elements of G that appear in (6.8) and thus obtain a *new* function $U(k_m)$. Self-consistency requires that the new $U(k_m)$ should agree with the original one.

The definition of $U(k_m)$ which we have just given removes many diagrams from consideration and has always been used in the theory of nuclear matter. We may now ask whether or not it is desirable to cancel this particular sequence of diagrams. If the expansion were convergent in powers of G , then summing all diagrams through n th order should give a more accurate result than summing only through the $(n-1)$ st order. But the sum in the present case is over specially selected diagrams of 3rd, 4th, 5th, \dots , order, and there is no *a priori* reason to expect this procedure to improve our estimate for the energy; one can easily conceive of getting a less accurate result by this means.

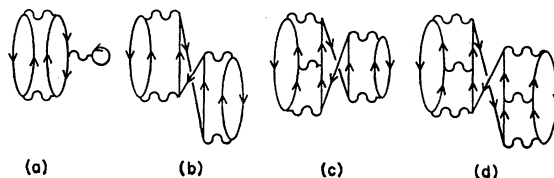


FIG. 29. Some of the G -matrix diagrams, with conventional energy denominators, that come from the v -matrix diagrams of Figs. 28(a), (b).

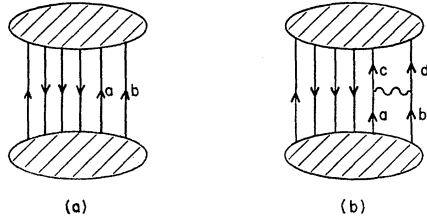


FIG. 30. Diagrams used to calculate the effect of inserting a G matrix between particle lines. (a) An arbitrary diagram in the Brueckner-Goldstone expansion. (b) The same diagram with a G matrix inserted between two particle lines, thus leaving the number of hole lines unchanged.

Another way of investigating the desirability of canceling this particular sequence of diagrams is to note that if the expansion in powers of G is rapidly convergent, then the inclusion or omission of a few fourth-order and higher terms should make little difference. However, in the present case it makes a *great* difference. If only the third-order diagram of Fig. 26(a) were included in the definition of $U(k_m)$, then the middle G matrix would be off the energy shell by the amount $(E_a + E_b - E_l - E_m)$, which is typically 600 to 800 MeV. The parameter γ^2 , defined by Eq. (5.18), would then be about $20 F^{-2}$ —ten times its typical on-energy-shell value. The core volume and core boundary terms in Eq. (5.41) for the G matrix would become much larger, while the attractive outer term would not change much. As a result, $U(k_m)$ would be repulsive instead of strongly attractive. This is an indication that the expansion in powers of G does *not* converge well. It will now be made plausible that this is indeed the case.

Consider an arbitrary diagram which at some level has two upgoing lines labeled a and b , as shown in Fig. 30(a). The blobs in this picture are supposed to represent the upper and lower parts of the diagram. By inserting a G matrix between lines a and b , as shown in Fig. 30(a), we obtain a new diagram whose order exceeds that of the original diagram by one. To get an idea of how well the expansion in powers of G converges, we would like to compare the contribution of the new diagram with the contribution of the old one. Because of the additional G matrix in diagram (b), the contribution of (b) is $-\sum_{c,d>A} \langle cd | (1/e)G | ab \rangle$ times that of (a). In addition, the upper blob of the new diagram is different from the upper blob of the old one because the incoming lines a and b have been changed to c and d . To obtain a rough estimate, we neglect this latter difference between the diagrams and thereby obtain

Contribution of Fig. 30(b) to energy

Contribution of Fig. 30(a) to energy

$$\approx - \sum_{c,d>A} \langle cd | e^{-1}G | ab \rangle. \quad (6.9)$$

In order to evaluate this quantity, we first replace it

by the equivalent expression

$$- \sum_{\text{all } pq} \langle pq | (Q/e)G | ab \rangle. \quad (6.10)$$

Then, using (4.10), we note that

$$\Phi_{pq}(\mathbf{r}=0, \mathbf{R}) = \Omega^{-1} \exp(i\mathbf{K}_{pq} \cdot \mathbf{R}). \quad (6.11)$$

Now, as we sum over p and q , \mathbf{K}_{pq} must remain constant and equal to \mathbf{K}_{ab} . It therefore follows from (6.11) that

$$\Omega \exp(-i\mathbf{K}_{ab} \cdot \mathbf{R}) \Phi_{pq}(\mathbf{r}=0, \mathbf{R}) = 1. \quad (6.12)$$

Using this result along with the fact that

$$(Q/e) | ab \rangle = \Phi_{ab} - \Psi_{ab} = Z_{ab}, \quad (6.13)$$

we can easily evaluate expression (6.10). The result is

$$\begin{aligned} & - \sum_{\text{all } pq} \langle pq | (Q/e)G | ab \rangle \\ &= -\Omega \exp(-i\mathbf{K}_{ab} \cdot \mathbf{R}) \sum_{\text{all } pq} \Phi_{pq}(\mathbf{r}=0, \mathbf{R}) \langle pq | Z_{ab} \rangle, \\ &= -\Omega \exp(-i\mathbf{K}_{ab} \cdot \mathbf{R}) Z_{ab}(\mathbf{r}=0, \mathbf{R}), \\ &= -\Omega \exp(-i\mathbf{K}_{ab} \cdot \mathbf{R}) \Omega^{-1} \exp(i\mathbf{K}_{ab} \cdot \mathbf{R}) \zeta_{ab}(\mathbf{r}=0), \\ &= -\zeta_{ab}(\mathbf{r}=0) = -1. \end{aligned} \quad (6.14)$$

Thus the new diagram, with the next higher power of G , is just as large as the old one. It is therefore evident that an expansion in powers of G is very unlikely to converge. This result is clearly attributable to the infinitely repulsive core, which causes $\psi_{ab}(\mathbf{r})$ to vanish inside the core and thus leads to $\zeta_{ab}(\mathbf{r}=0) = 1$.

Inserting a G matrix between two particle lines does not reduce the size of a diagram, but the situation is different if one of the lines is a hole line. Consider, for example, the effect of attaching a bubble interaction to a particle line, as shown in Fig. 31. The ratio of the contribution from the new diagram to that from the old one is exactly equal to

$$\sum_{n \leq A} \langle bn | (1/e)G | bn \rangle,$$

which can be approximated by

$$\begin{aligned} \sum_{n \leq A} \langle bn | e^{-1}G | bn \rangle &= \sum_{n \leq A} \Omega^{-1} \langle \mathbf{k}_{bn} | e^{-1}G | \mathbf{k}_{bn} \rangle \\ &\approx \sum_{n \leq A} \Omega^{-1} \langle \mathbf{k}_{bn} | \zeta_{bn}^R \rangle. \end{aligned} \quad (6.15)$$

The summation over n is carried out by multiplying

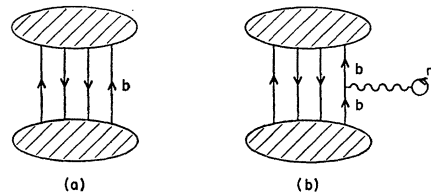


FIG. 31. Diagrams used to calculate the effect of inserting a bubble interaction into a particle line. (a) An arbitrary diagram in the Brueckner-Goldstone expansion. (b) The same diagram with a bubble interaction inserted into a particle line, thus increasing the number of hole lines by one.

by the number of particles A and replacing $\langle \mathbf{k}_{bn} | \zeta_{bn}^R \rangle$ by its value for some "average state" n in the Fermi sea. Since A/Ω is equal to the particle density ρ , the result is

$$\rho \int \exp(-i\mathbf{k}_{bn} \cdot \mathbf{r}) \zeta_{bn}^R(\mathbf{r}) d^3r. \quad (6.16)$$

The integrand is unity for $r \leq c$ and rapidly goes to zero for $r > c$, and a typical value for the integral is $4\pi c^3$. Therefore the insertion of a bubble into a particle line multiplies the contribution from the diagram by the factor

$$\rho 4\pi c^3 = 3(c/r_0)^3 = 0.14 \quad (\text{for } c = 0.4 \text{ F, } r_0 = 1.12 \text{ F}), \quad (6.17)$$

where the average interparticle spacing r_0 is defined by Eq. (1.4).

These estimates indicate that the size of the contribution from a diagram is *not* determined by the number of G matrices it contains. Rather, it depends on the number of hole lines. Putting an extra hole line into a diagram reduces its magnitude by the factor $3(c/r_0)^3$, which is considerably less than one. Therefore it is sensible to group diagrams, not according to powers of G , but according to the number of hole lines. This leads to an expansion in powers of the density because the expansion parameter $3(c/r_0)^3$ is proportional to ρ .

As we have seen, the hard core plays the dominant role in these estimates. The assumption of the hard core leads to $\psi = 0$ and $|\zeta| = 1$ at small distances, and this fact is responsible for the divergence of an expansion powers of G . However, we have also made use of the weakness of the attractive part of the potential. For example, in estimating the integral in formula (6.16), it was important to know that ζ goes rapidly to zero outside the repulsive core. This rapid decay of ζ occurs only because the attractive part of v is not too strong.

The grouping of diagrams according to number of hole lines corresponds to the following very simple physical idea. Two particles are strongly correlated, in the sense that ψ differs appreciably from ϕ , only when the distance between them is less than some "correlation length" which is of the order of c or only a little larger. Within a sphere of radius r_0 centered on any particular particle, there will be on the average one other particle. The probability that this other particle is close enough to the first one to be strongly correlated with it is of the order of $(c/r_0)^3$. Thus the probability of strong two-body correlations is proportional to $(c/r_0)^3$. Similarly, the probability of three-body correlations is of order $(c/r_0)^6$, and so on. Therefore, an expansion in which the first term is the energy due to two-body correlations, the next is from three-body correlations, etc., is characterized by an expansion parameter $(c/r_0)^3$ and should converge well. This is just the type of expansion obtained by grouping the dia-

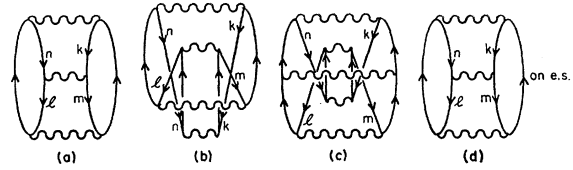


FIG. 32. A sequence of diagrams each of which contains three independent hole lines. Diagrams (a), (b), (c) are the first three members of the sequence. The sum of this sequence is the hole-hole diagram (d), with the middle G matrix calculated on the energy shell.

grams according to the number of hole lines. The diagrams with n independent hole lines represent the energy arising from n -body correlations.

The hole-line expansion converges because the "correlation length" is much less than the interparticle spacing r_0 . And this condition is satisfied because the nucleon-nucleon potential fulfills two essential requirements: (1) the core radius c is small compared to r_0 and (2) the nuclear attraction is so weak that the range of the strong correlations is characterized by the core radius, *not* by the range of the attractive force (which is somewhat larger than r_0).

Let us now consider in detail the classification of diagrams according to the number of hole lines. Each of the first-order G -matrix diagrams shown in Fig. 16 has two hole lines, and all other diagrams have at least three hole lines. So the first-order G -matrix diagrams represent the leading term in the expansion in powers of density.²⁷

There are three distinct classes of diagrams with three independent hole lines. One of these is the sequence of diagrams (Fig. 29) that is canceled by our choice of $U(k_m)$. Each of these diagrams has four hole lines, but two of the hole lines have the same momentum, so that only three are independent. This answers our question about whether or not it is sensible to cancel this particular sequence of diagrams by means of $U(k_m)$. It is sensible because each of these diagrams has three independent hole lines, and they should therefore be grouped together and treated as a single term. This important term, which gives a positive contribution of 6–8 MeV per particle, is then exactly canceled by our choice of $U(k_m)$.

A very similar class of three-hole-line diagrams is shown in Fig. 32 (exchange diagrams omitted). Although each diagram contains four hole lines, only three of the hole momenta are independent because momentum conservation requires that $\mathbf{k}_l + \mathbf{k}_m = \mathbf{k}_n + \mathbf{k}_k$. The sequence of diagrams whose first three members are shown in Fig. 32(a), (b), (c), is exactly summed by evaluating the hole-hole interaction diagram of Fig. 32(d), with the middle G matrix calculated on the energy shell—much as in the case illustrated in Fig. 29.

²⁷ This fact was first pointed out by N. M. Hugenholtz, *Physica* 23, 533 (1957).

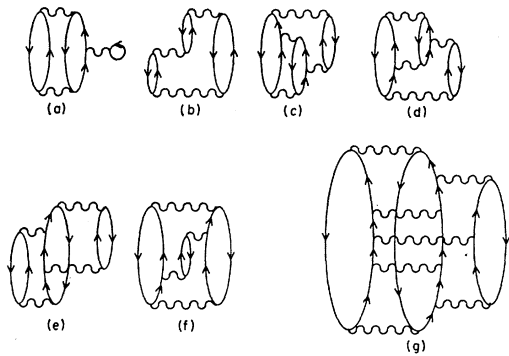


FIG. 33. Some of the three-hole-line diagrams studied by Bethe, as explained in the text.

The contribution from diagram 32(d) is comparable in magnitude to that from the hole-bubble diagram of Fig. 28(c) except for three statistical factors¹⁹: (1) The contribution from diagram 32(d) contains a factor $\frac{1}{2}$ from the restriction to distinct matrix elements in formula (2.9) for H_1 . [This point was discussed in connection with Fig. 3 and Eq. (2.13)]. (2) For a spin-independent potential, every line in a given closed loop, whether upgoing or downgoing, must correspond to the same single-particle spin and isotopic spin state. Therefore, diagram 28(c) involves three independent spin-isospin states, but 32(d) involves only two. Since there are four possible spin-isospin states for a single particle, the statistical weight of diagram 32(d) is $\frac{1}{4}$ that of 28(c). (3) Suppose that in diagram 32(d) we decide to sum over $\mathbf{k}_l, \mathbf{k}_m, \mathbf{k}_n$, allowing \mathbf{k}_k to be determined by momentum conservation. Then $\mathbf{k}_k = \mathbf{k}_l + \mathbf{k}_m - \mathbf{k}_n$ must be *in* the Fermi sea. Hence the possible choices of $\mathbf{k}_l, \mathbf{k}_m, \mathbf{k}_n$ are limited by the requirement that $|\mathbf{k}_l + \mathbf{k}_m - \mathbf{k}_n| < k_F$. From this Rajaraman¹⁹ shows that the phase-space factor for diagram 32(d) is $\frac{1}{8}$ that for 28(c). (Note that the three-hole momenta in 28(c) can range independently over the Fermi sea.) Because of these three factors, the contribution from the hole-hole diagram is only about $\frac{1}{8}$ that from the hole-bubble diagram, and in practice the hole-hole diagram is ignored.

The first few members of the third class of three-hole-line diagrams are shown in Fig. 33 (exchange diagrams omitted). There are 2 diagrams of third order in G , 4 diagrams of fourth order, 8 of fifth order, etc. The general structure is illustrated by the seventh-order diagram of Fig. 33(g). The first two interactions produce three particle lines and three hole lines. Then interactions are inserted in all possible ways between the particle lines, except that two successive interactions between the same pair of particle lines is not allowed. Only the particle lines can participate in these interactions; otherwise we would get more than three hole lines. Finally, the last two interactions in the diagram carry the system back to the state with no particles and no holes.

It was in studying this sequence of diagrams that

Bethe²¹ was led to the conclusion that the expansion in powers of G is divergent, a result which was already suggested by the work of Rajaraman.²⁰ A detailed treatment of these diagrams is given in the following article,² but it seems appropriate to summarize the main results here.

Bethe²¹ demonstrated explicitly that the contributions from the sequence of diagrams of Fig. 33, when summed order by order, form a divergent series. He found the divergence of the series to be a direct result of the fact that $|\zeta|$ is large for small r . In fact, the series turns out to be divergent whenever $|\zeta| > \frac{1}{2}$ at small distances.

To get sensible results, one must sum the divergent series by means of an integral equation; there is no way to collapse this class of diagrams to a single diagram, as was done for the other three-hole-line diagrams. The procedure is analogous to that by which ladders of v matrices are summed to a G matrix. When v contains a strong repulsion, the series $v - v(Q/e)v \dots$ is certainly divergent. Nevertheless, this series can be formally summed to obtain the G matrix, which is finite and well-defined, and which satisfies the integral equation $G = v - v(Q/e)G$. In a similar way, one can write an integral equation for the sum of the three-hole-line diagrams, and this equation will have a finite and meaningful solution.

Since the G matrix represents the interaction of a pair of particles, the integral equation for G leads to a two-body Schrödinger equation. The three-hole-line diagrams of Fig. 33, however, represent contributions to the energy from three-particle correlations. Therefore the integral equation which sums these diagrams is equivalent to a *three-body* Schrödinger equation.

This three-body equation is called the Bethe-Faddeev equation. By obtaining an approximate solution to this equation, Bethe showed explicitly that the three-body energy is smaller than the two-body energy by a factor of order $(c/r_0)^3$. A numerical calculation, recently completed by Kirson,^{28,29} gives -5 MeV per particle for the three-body energy. This is satisfactorily small in comparison with the contribution of about -35 MeV per particle from the two-hole-line diagrams, and it is reasonable to expect the corresponding four-body diagrams to contribute less than 1 MeV per particle.

This completes the discussion of all the diagrams that have either two or three independent hole lines. The two-hole-line diagrams are just the first-order G -matrix diagrams. There are three distinct classes of diagrams with three independent hole lines. In the first class are the diagrams of Fig. 29, which are canceled by our choice of $U(k)$ for $k < k_F$. Next there is the numerically unimportant hole-hole interaction of Fig. 32. Finally, there is the class of diagrams shown in Fig. 33, which was studied by Bethe in his work on three-body correlations. There are many classes of four-hole-line

²⁸ M. W. Kirson, Nucl. Phys. A99, 353 (1967).

²⁹ A more accurate treatment may well give a three-body energy which is much closer to zero, or even slightly positive (private communication from H. A. Bethe).

diagrams, but they are presumably negligible, and no one has studied them.

Let us now discuss very briefly the choice of $U(k)$ for $k > k_F$. In analogy with Hartree-Fock theory, we might try to choose $U(k_b)$ in such a way that the three diagrams shown in Fig. 34 cancel out. But this is a bad choice because, as we have seen, the particle-bubble diagram 34(a) is just one of an infinite series of diagrams which are all equally important. The sum of this series is -5 MeV per particle, while the particle-bubble diagram by itself contributes roughly $+5$ or $+6$ MeV per particle. Thus the Hartree-Fock method amounts to splitting a term of -5 MeV into two terms of $+5$ and -10 MeV and canceling the $+5$ MeV term by an appropriate choice of $U(k_b)$, while leaving the -10 MeV term unaccounted for. This is the procedure that was actually used before the correct treatment of three-body correlations was understood.^{18,30,31} As would be expected from the preceding discussion, it gave a binding energy that was considerably too small.

There are at least two sensible choices for $U(k_b)$. If the three-hole-line diagrams of Fig. 33 are calculated explicitly, then all nonnegligible diagrams are taken into account without any help from $U(k_b)$. In this case we may simply take $U(k_b) = 0$.^{32,33} On the other hand, it is possible to choose $U(k_b)$ in such a way that diagram 34(c) cancels *all* the three-body diagrams of Fig. 33. Since the question of $U(k_b)$ is treated in detail in the following article,² the discussion will be dropped at this point.

With these methods of calculating the energy per particle of nuclear matter, the value implied by any particular realistic nuclear force is believed to be obtainable to high accuracy. One can calculate just the first-order diagrams, with $U(k_m)$ defined by Eq. (6.8), and with $U(k_b)$ chosen so as to cancel all the three-body diagrams of Fig. 33. At this point, the only terms left out are the hole-hole diagram and diagrams with four or more independent hole lines; the total contribution of these should be less than 1 MeV per particle.

Detailed calculations have been made in this way by Sprung, Bhargava, and Dahlblom²² and by Sprung and Bhargava.²³ The calculations were done with the

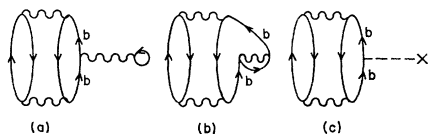


Fig. 34. Diagrams involved in the Hartree-Fock definition of $U(k_b)$ for nuclear matter.

³⁰ K. A. Brueckner and K. S. Masterson, *Phys. Rev.* **128**, 2267 (1962).

³¹ M. Razavy, *Phys. Rev.* **130**, 1091 (1963).

³² This procedure has been followed by N. Azziz, *Nucl. Phys.* **85**, 15 (1966). However, Azziz did not evaluate the three-body diagrams.

³³ A very detailed treatment, which leads in first approximation to this procedure, is given by B. H. Brandow, *Phys. Rev.* **152**, 863 (1966).

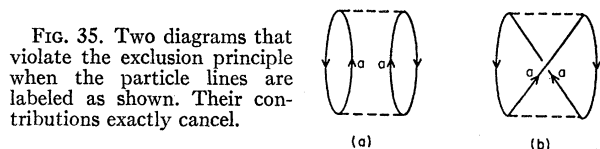


Fig. 35. Two diagrams that violate the exclusion principle when the particle lines are labeled as shown. Their contributions exactly cancel.

nucleon-nucleon potentials of Reid,³⁴ of Hamada and Johnston,³⁵ and of Bressel.³⁶ Each of these potentials fits the scattering data very well up to 300 MeV. The first two have hard cores, but the Bressel potential has a core of finite height. Unfortunately the results of Ref. 22 are based on an incorrect application of Bethe's three-body theory.³⁷ When the mistake is corrected, the binding energy is reduced by about 6 MeV per particle,³⁷ and the good agreement between theory and experiment shown in Ref. 22 is destroyed. According to Bethe,³⁷ this result makes it almost certain that a potential with a *hard* core (and which fits the scattering data) cannot give the correct binding energy and equilibrium density for nuclear matter.

However, several investigations^{21,23,38} indicate that better results can be obtained by using a potential that has a more realistic repulsion of Yukawa shape. Reid has developed a potential of this type which gives an excellent fit to the scattering data,³⁷ and it is planned to use this potential in nuclear-matter calculations.^{37,39}

ACKNOWLEDGMENTS

The author is grateful to H. A. Bethe and R. Rajaraman for their encouragement to prepare this report for publication. He is also indebted to the Physics Division of Argonne National Laboratory (in particular to F. Coester and M. Peshkin) for the opportunity to give several talks on nuclear matter. Most of the material in this article was first presented in these informal talks at Argonne.

APPENDIX A. THE EXCLUSION PRINCIPLE IN INTERMEDIATE STATES

The Pauli exclusion principle in intermediate states was ignored for simplicity in Sec. II. But since it must be understood by anyone who wants to apply the Goldstone theory, it will be briefly treated here.

Let us consider the diagram of Fig. 35(a), restricting our attention to the case in which both upgoing lines represent the same single-particle state a . The rules of Table I imply a nonzero contribution to the energy from this diagram. On the other hand, the intermediate Slater determinant in this diagram has two particles in state a , and any such Slater determinant is identically zero. So the actual contribution of Fig. 35(a) is zero. The same result follows from the second-quantization

³⁴ R. V. Reid (private communication).

³⁵ T. Hamada and I. D. Johnston, *Nucl. Phys.* **34**, 382 (1962).

³⁶ C. Bressel, Ph.D. thesis, Massachusetts Institute of Technology, 1965.

³⁷ H. A. Bethe (private communication).

³⁸ This possibility was first investigated by C. W. Wong, *Nucl. Phys.* **56**, 213 (1964); **71**, 385 (1965).

³⁹ D. W. L. Sprung (private communication).

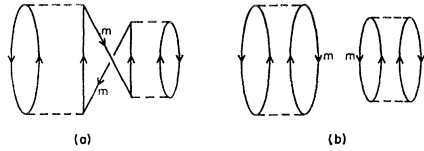


FIG. 36. Two exclusion-violating diagrams whose contributions cancel. Diagram (a) is included in the Goldstone expansion, but (b) is not.

formalism because the Fermion operators give a factor $\langle \Phi_0 | a_l^\dagger a_m^\dagger a_a a_a a_a^\dagger a_a^\dagger a_m a_l | \Phi_0 \rangle$, and this is zero because $a_a^2 = 0$. Thus it appears that correct results can be obtained only if the sum over intermediate states is restricted so as to exclude Slater determinants that have two particles or two holes in the same single-particle state.

However, this problem can be handled in a more convenient way. Consider diagram 35(b), which is identical with 35(a) except for exchange of the two particle lines having the same label. For 35(b) the diagram rules give a spurious contribution that exactly cancels the spurious contribution from 35(a). This sort of cancellation is completely general. Thus if all the diagrams of a given order (both connected and disconnected) are evaluated according to the rules of Table I, then all the spurious diagrams cancel out and the final result is correct. This fact is expressed by saying that the Pauli principle may be neglected in intermediate states.

A more interesting aspect of this situation is illustrated in Fig. 36. Diagrams 36(a) and 36(b) both are said to violate the Pauli principle because each one has two hole lines m at the same level; their contributions exactly cancel. But diagram 36(b) is disconnected and therefore does not appear in the Goldstone expansion. The question then arises of whether or not the corresponding connected diagram 36(a) should be included in the Goldstone series.

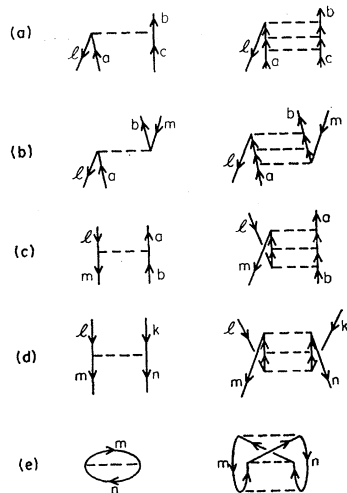


FIG. 37. Some examples of ladder diagrams that occur in the definition of the G matrix, as explained in Appendix B.

Goldstone's derivation⁹ shows that diagram 36(a) *should* be included in the Goldstone expansion. This diagram gives a nonzero contribution to the energy that is determined by the rules of Table I, and its contribution is not canceled by any other term in the expansion.

The general result is that *every* connected diagram must be included in the Goldstone expansion, even if it violates the Pauli principle and is not canceled by any other connected diagram. Each such diagram gives a nonzero contribution to the energy that is computed by the methods described in Sec. II. This result is surprising at first sight. To see how it comes about, the reader is referred to the Goldstone⁹ paper. A physical interpretation of the exclusion-violating diagrams is given in Sec. 8 of Ref. 13.

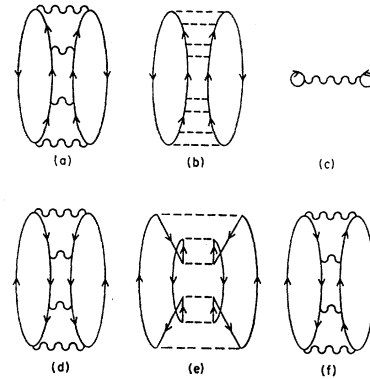


FIG. 38. Illustration of the difference between the redundant ladder diagram (a) and the legitimate diagrams (d) and (f). A detailed discussion is given in the text of Appendix B.

APPENDIX B. MORE DETAILS ON THE TRANSFORMATION FROM ν TO G

This appendix, which supplements Sec. III, gives a number of relationships among diagrams. These are supposed to give the reader a better understanding of how the Brueckner-Goldstone expansion is obtained from the Goldstone expansion.

To any ν interaction corresponds a unique sequence of ladders whose sum is a G interaction. The correct sequence of ladders is the one that reproduces the terms in expression (3.7). In Fig. 37 are drawn a number of ν interactions, and beside each one is shown the third-order ladder in the sequence that converts the ν to a G .

In Fig. 38, diagram a is redundant because it corresponds to ladders of the sort shown in b , and all such ladders are already included in (c). Diagram (d), however, has repeated G -matrix interactions between *hole* lines, not between particle lines. So diagram (d) is not redundant; one of its corresponding ladder diagrams is diagram (e), which is not contained in any G -matrix diagram of less than fourth order. Similarly, diagram (f) is legitimate and occurs in the Brueckner-Goldstone expansion.